Compositional relations in Li-micas from S.W. England and France: an ion- and electron-microprobe study

C. M. B. HENDERSON, JOANNA S. MARTIN

Department of Geology, The University, Manchester M13 9PL

AND

R. A. MASON*

Department of Earth Sciences, University of Cambridge, Cambridge CB2 3EQ

Abstract

A combination of ion-microprobe (for Li) and electron-microprobe (for other major elements including F) methods has been used to analyse Li-rich micas from the S.W. England batholith (mainly the St Austell granite) and the Massif Central, France. Rocks showing various degrees of hydrothermal alteration were studied in order to separate the original compositional trends from alteration trends. The original compositional trend is essentially one of increasing Li with increasing degree of evolution. The main atomic substitution in the original micas is 3Li substituting for Al and 2 vacancies in octahedral sites; substitution of Li for R^{2+} (Fe, Mn, Mg) in octahedral co-ordination is generally subordinate. Alteration trends involve a loss of Li, Fe, F, Rb and Cs, and a gain in Al. The effects of volatile elements on phase relations of granites are reviewed and it is concluded that the original Li-micas were primary, i.e. crystallized from the melt. It is suggested that the late-magmatic stage passed transitionally into the hydrothermal stage leading inevitably to subsolidus recrystallization (autometasomatism) of the primary minerals, so introducing further textural and mineralogical complexities to the rocks.

KEYWORDS: Li-micas, ion-microprobe, electron-microprobe, S.W. England, France.

Introduction

THE occurrence of Li-rich micas is generally restricted to differentiated 'late-stage' granites and pegmatites, and to their associated metasomatic rocks. Based on bulk chemical analyses of separated minerals, Foster (1960) described compositional trends for Li-micas from worldwide localities and deduced substitution mechanisms. Two series were identified. Firstly, an essentially iron-free series from lithian muscovite towards trilithionite (ideal formula,

$$K_2(Al_3Li_3)^{VI}[Al_2Si_6]^{IV}O_{20}(OH,F)_4),$$

and polylithionite,

$$(K_2(Al_2Li_4)[Si_8]O_{20}(OH,F)_4);$$

this series contains an immiscibility gap. Secondly, an Fe-bearing series showing essentially complete solid solution from siderophyllite,

$$(K_2(Fe_4^{2+}Al_2)[Al_4Si_4]O_{20}(OH,F)_4),$$

through zinnwaldite,

$$(K_2(Li_2Fe_2^{2+}Al_2)[Al_2Si_6]O_{20}(OH,F)_4),$$

towards polylithionite. Rieder (1970) confirmed the latter trend using chemically analysed micas from Czechoslovakia. The high-Li micas in both the low- and high-Fe series are 'lepidolites'. Li and F show a well-developed, positive correlation in the muscovite–lepidolite series (Foster, 1960) but this correlation in the Fe-rich series (Rieder, 1970) is rather less well developed. The above

* Present address: Department of Earth Sciences, Memorial University of Newfoundland, St John's, Newfoundland, Canada A1B 3X5.

Mineralogical Magazine, September 1989, Vol. 53, pp. 427–449

relationships are discussed in recent reviews by Hawthorne and Černý (1982) and Černý and Burt (1984). Very recently Stone *et al.* (1988) have combined bulk chemical analyses with microprobe data for trioctahedral micas from the Cornubian batholith, S.W. England. They confirmed the continuous solid-solution series from siderophyllite to lepidolite. They also redefined the compositional boundaries between siderophyllite and zinnwaldite and between zinnwaldite and lepidolite as occurring at $Li_{30}R^{2+}_{70}$ and $Li_{70}R^{2+}_{30}$ respectively; this classification scheme is used in the present paper.

It is well known that granitic rocks which contain Li-micas almost invariably show effects of subsolidus hydrothermal alteration, sometimes pervasively. Indeed, some authors believe that late-crystallized generations of Li-micas may be hydrothermal rather than primary (e.g. Stone, 1984; Manning and Exley, 1984). Even apparently fresh Li-micas frequently show incipient alteration along cleavages. Under these circumstances bulk chemical analyses may not accurately reflect the compositions of the original micas and, in addition, intra-crystal zoning trend information is not available. The latter data would be invaluable for deducing element substitution mechanisms. Although electron-microprobe analyses yield zoning trends for other elements (cf. Stone *et al.*, 1988), Li cannot be detected by this technique.

We have used a combination of ion- and electron-microprobe analyses to analyse Li-micas in Hercynian granites from S.W. England and the Massif Central, France. Micas from rocks showing variable degrees of hydrothermal alteration were studied in order to distinguish the original chemical features of the micas from hydrothermal alteration trends. The data are used to discuss substitution mechanisms, to revise petrological interpretations, and to assess whether the original (unaltered) Li-rich micas are truly primary, or

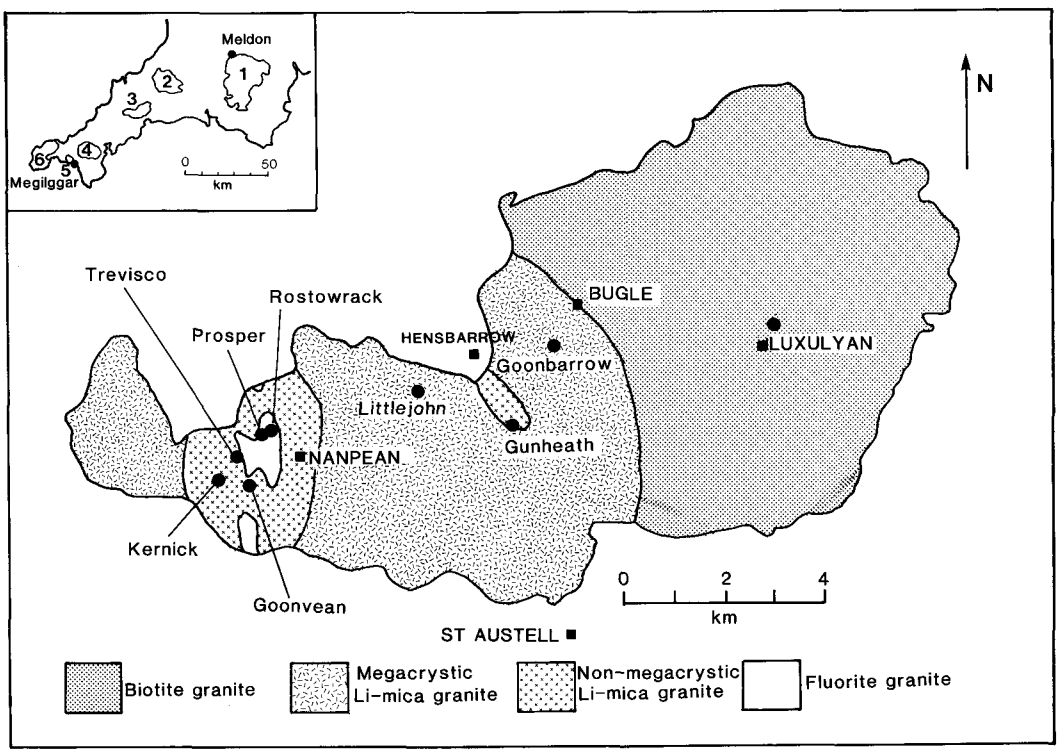

FIG. 1. Geological sketch map of the St Austell granite, S.W. England (after Exley and Stone, 1982), showing the different rock units. The localities where samples were collected are shown by solid round spots (also in the inset map); see Appendix for full listing of sample numbers. The different granite bodies in the inset map are identified by: 1 Dartmoor; 2 Bodmin Moor; 3 St Austell; 4 Carnmenellis; 5 Tregonning–Godolphin; 6 Lands End.

formed under sub-solidus conditions during the earliest stages of hydrothermal activity.

Rock samples studied

Exley and Stone (1982) have reviewed the geology of the S.W. England granite batholite and much of their terminology is adopted here. Most of the S.W. England samples described in the present paper are from the St Austell granite (Fig. 1) but two from the Meldon aplite and one from the Megiliggar Rocks locality in the Tregonning–Godolphin granite were also studied (inset to Fig. 1). The St Austell granite consists essentially of three units: biotite granite (denoted BG) which characteristically contains megacrysts of alkali feldspar; megacrystic Li-mica granite (MLG); and non-megacrystic Li-mica granite (NMLG). The distribution of these units is shown in Fig. 1. Hill and Manning (1987) recently remapped the MLG between Bugle and Nanpean (Fig. 1) and showed that this unit is more petrographically variable than had been recognized before, containing both megacrystic and equigranular biotite granites as well as tourmaline- and Li-mica-bearing granites. Manning (1988) and Manning and Hill (in press) refer to the NMLG as 'topaz granite' and suggest that the western and eastern exposures in the St Austell granite ('Nanpean and Hensbarrow stocks' respectively, Fig. 1) are connected at depth. The St Austell samples studied in the present work include biotite granites, megacrystic Li-mica granites, and non-megacrystic Li-mica granites and include unaltered types as well as the altered varieties fluorite granite and chinastone (Exley and Stone, 1982).

Samples from the Massif Central, France, are from the Echassières (Beauvoir) and Montebras granites (Aubert, 1969). Localities for both the English and French samples are given in Appendix I and significant information concerning the mica texture and alteration effects are summarized below.

S.W. England

Biotite granite unit. (Type B of Exley and Stone, 1982). Sample 5007 is from the main BG unit (Luxulyan, Fig. 1) and is a typical Cornubian biotite granite. Biotite forms flakes <2 mm across while muscovite is present as an interstitial phase (2 mm). Neither of these micas show any textural signs of having formed by replacement of an earlier phase and both are considered to be primary. Accessory minerals include brown tourmaline and apatite. Hydrothermal alteration effects are mainly restricted to clouding of the orthoclase perthite with associated development of sericite.

Megacrystic Li-mica granite unit. (Type D). Sample 5089 is from Goonbarrow (Fig. 1) within the MLG but is petrographically very similar to BG 5007. The other samples studied contain interstitial regions of Li-rich, Fe-poor mica (<2 mm) which is either pale pink–brown (samples 5096 and 5106) or almost colourless (samples 5011, 5024 and 5093). Accessory brown tourmaline and apatite are ubiquitous and some samples contain topaz. Using the Hill and Manning (1987) classification, 5089 is a biotite granite (and is treated as a BG in further discussion); 5011, 5024, 5093 and 5096 are tourmaline granites; and 5106 is a globular quartz granite. The rocks studied here show effects of hydrothermal alteration varying from those with essentially unaltered micas coexisting with slightly clouded feldspars to those with partially altered and recrystallized micas. The main petrographic feature of altered micas is the presence of fluorite along mica cleavages. Such micas coexist with deeply clouded feldspars altered to sericite. The order of increasing degree of hydrothermal alteration is: 5089, 5093 → 5024 → 5011 → 5106 → 5096. The unaltered interstitial Li-rich micas show no signs of having formed by replacement of earlier phases and there is no textural evidence to suggest that they are not primary. However, at this stage we prefer to describe them as the original micas to crystallize.

Non-megacrystic Li-mica granite unit (Type E, Exley and Stone, 1982) *and fluorite granite* (Type F). The mica present in these rocks is invariably in interstitial patches (<2 mm) with the unaltered Li-rich types again showing no signs of having replaced an earlier phase. Topaz and apatite are ubiquitous but tourmaline is rare. The petrographic features of altered mica and the range of hydrothermal alteration effects in these rocks are similar to those described for the megacrystic Li-mica granites except that, in the most altered types, topaz is pervasively replaced by aggregates of sericite. The highly altered rocks (chinastones) tend to have fluorite present in interstitial patches (<$\frac{1}{2}$ mm), as well as within micas. Vermicular fluorite stringers are also present along quartz and feldspar grain boundaries. The order of increasing degree of hydrothermal alteration is: 5001 → 5020 → 5015, 5022, 5031, 5081 → 5080, 5085 → 5005 → 5017.

Aplites. Two samples from the Meldon aplite (5003, 5016) and one from the Megiliggar Rocks (5100) were studied. All have subhedral flakes of Li-rich mica (<1 mm) which show no textural signs of a replacement origin. These micas show only slight alteration while feldspars are generally deeply clouded. Alteration effects increase in the order 5016 → 5100 → 5003.

Massif Central, France

'Lepidolite' granites. Three samples from Beauvoir, Échassières (5050, 5052, 5054) all show feldspars which are almost totally altered to sericite and clay minerals. Colourless Li-rich mica flakes (<1 mm) seem to be recrystallizing from fine-grained mica (Li-poor muscovite) intergrowths and are clearly secondary phases. The sample from Montebras (5062) is much less altered and contains a pale cream Li-rich mica (<1 mm), showing slight patchy alteration, coexisting with clouded feldspar (mainly albite) and associated sericite. This Li-rich mica shows textural relations consistent with it being primary.

Analytical methods and data recalculation

Electron-microprobe analyses. Standard, 30 μm thick polished and carbon coated sections were firstly analysed by electron-microprobe in the Geology Department, University of Manchester (Cameca Camebax fitted with two wavelength-dispersive (WD) spectrometers and a Link Systems 860–500 energy-dispersive (ED) detector). On some samples F was analysed by WD and the other elements by ED methods; in others Si, F, Rb and Cs were determined by WD. Spectral interference between Si and Rb necessitated the use of WD for high Rb micas in particular. Natural fluorite was used as a standard for F, natural pollucite for Cs, and a synthetic glass for Rb. A defocused beam of 5–10 μm diameter was used to minimise loss of F and alkali elements.

Ion-microprobe analyses. In the ion-microprobe technique an ion beam (primary beam) is focused on the polished surface of a sample and used to erode ('sputter') material from the target. In the sputtering process, ions (secondary ions) characteristic of the sample are produced and can be focused on the entrance slit of a mass spectrometer, whence both isotopic and elemental analyses are possible.

The analyses were performed with a modified AEI-IM20 instrument (Banner and Stimpson, 1974; Long *et al.*, 1980). The following instrumental conditions were used: accelerating voltage 20 kV; primary beam current 13–15 nA; beam diameter 10–15 μm; bombarding species $^{16}O^-$; positive secondary ions collected.

For elemental analysis the problems to overcome are the presence of interfering species in the mass spectrum and the conversion of count rates to concentrations.

Mass spectral interferences can result from the presence of: isotopes of different elements at the same mass (e.g. Ca and K at mass 40); multiply charged ions (e.g. $^{27}Al^{3+}$ at mass 9); or molecular ions (e.g. $^{40}Ca^{16}O^+$ at mass 56). In the case of lithium the presence of interferences was sought by examining the mass spectrum at high mass resolution (i.e. $M/\Delta M = 6000$). No interferences were found. All analyses were, therefore, carried out at a mass resolution of approximately 400.

Placing the observed count rates on a concentration scale involves the use of standards. Ideally these should have a major element composition similar to the unknown because matrix compositions can affect ion yields. In the case of Li, however, Jones and Smith (1984) have found that a single calibration is suitable for all micas, indicating that significant matrix effects are absent. The standard used was a zinnwaldite from Virginia, USA supplied by Manchester museum. This material was chemically analysed for Li, and (OH) estimated from an infrared spectrum. All other elements were determined by electron microprobe giving the composition (wt.%) (1σ values in parentheses): SiO_2 46.4 (0.65), TiO_2 not detected (n.d.), Al_2O_3 20.9 (0.3), FeO 9.1 (0.26), MnO 3.9 (0.15), MgO n.d., CaO n.d., Li_2O 3.39, Na_2O 0.8 (0.11), K_2O 9.7 (0.13), F 7.0 (0.4), H_2O^+ 0.71, minus F ≡ O = 98.95. The generally low standard deviations in the electron probe results are consistent with the standard being homogeneous.

Following electron probe analyses the carbon coat was removed from the samples and standards which were ultrasonically cleaned and coated with gold. (In ion probe analysis gold is usually to be preferred to carbon as a conductive coating because it does not contribute to the mass spectrum in the region of interest in most silicate analyses.)

Spot positions analysed by electron microprobe were either marked on photographs or detailed drawings which were used to locate the ion beam so that Li analyses were made as close as possible to the electron probe analyses. Before each sample analysis counts were collected on the standard. For both sample and standard the ^7Li and ^{28}Si peaks were counted, using counting times of 1 sec, in the sequence Li–Si–Si–Li. The minor isotope ^7Li was chosen in preference to ^6Li when monitoring the standard to avoid damage to the detector from high count rates. Silicon was monitored to allow for any instrument drift. Several passes were made and cumultative counts recorded for each location. Li counts were converted to concentrations using the equation:

$$C_{Li} = I_{Li}/I_{Si} \cdot C_{Si} \cdot 1/\varepsilon_{Li}$$

where C_{Li} = unknown Li concentration, I_{Li} and I_{Si} are count rates on the sample, C_{Si} = known Si concentration in the sample, ε_{Li} = (counts per

ppm for Li)/(counts per ppm for Si). In the case of alkali elements, particularly Li, the peak to background ratio is favourable (>500 000:1) and a detection limit of 10 ppb has been reported (Wilson, 1980).

Data recalculation. The wt.% Li_2O values from the ion probe were combined with the electron probe analyses from the same areas and the cell formulae recalculated to 22 oxygens. This recalculation basis assumes that the sum of OH, F and Cl equals 4 atoms, i.e. that no oxy-mica component is present. No other calculation basis was possible due to the presence of variable Al in 4-co-ordinated sites and because of incomplete occupancy of the octahedral and 12-co-ordinated sites. In some micas which are almost certainly relatively rich in Rb this element was not determined and Si was analysed by ED. Under these circumstances the Si value quoted is likely to be slightly high ($\leq$1% relative), leading to under estimation of Al^{IV} and over estimation of Al^{VI}. In addition the 12-co-ordinated cation site total will be too small (i.e. Rb, Cs not dermined). Even in mica analyses including Rb and Cs values, the 12-co-ordinated site totals less than 2 per formula unit. This deficiency could be due to the presence of unanalysed H_3O^+ (Levillain, 1980), NH_4^+ (Hall, 1988) or vacancies. These stoichiometric complexities result in there being no worthwhile basis for modelling Fe^{3+}:Fe^{2+} contents: the Fe is, therefore, reported as Fe^{2+} throughout. This is unlikely to lead to serious errors as the rock types studied are typical S-type granites, which are characteristically reduced (cf. Fe^{2+}:Fe^{3+} ratios in chemically analysed micas, especially those from Li-mica granites; Stone *et al.*, 1988).

A few samples were not analysed for Li by ion microprobe; however, reasonable Li_2O estimates could be made for these based on their average SiO_2, Al_2O_3 and F (wt.%) electron-microprobe analyses (see Results section and Fig. 2). Cell formulae, based on 22(O), were then calculated for these samples, incorporating the model Li_2O values with average electron probe data.

Results and discussion

Average mica analyses (and 1σ standard deviations) for each of the S.W. England granites studied are given in Table 1. Within the MLG and NMLG, the least altered rocks have micas with the highest Li contents while the most altered rocks tend to have low to very low Li (e.g. MLG 5096, NMLG 5080, 5085 and 5017; Table 1). In a few Li-rich samples, partially altered and secondary micas were also analysed and the averages for these mica populations are reported in Table 2; note that in one sample (5005), three groups of variously altered micas have been identified (Table 2: II, III and IV). Average analyses for French micas are given in Table 3. Representative microprobe spot analyses for S.W. England and French micas are included in Table 4.

The interstitial textures of most of the Li-rich micas in the S.W. England rocks make it very difficult to establish clear spatial compositional trends which can be interpreted as progressive zoning. Even if systematic compositional variations are present it is not easy to deduce the order of crystallization, as the mechanisms of growth must involve the movement of 'crystallization fronts' through the interstitial pore space with no objective way of deducing the original nucleation site(s) and the directions in which growth occurred. However, in a few cases it was possible to analyse single, separate mica flakes where growth might have been from the interior outwards. In such grains the margins are generally more enriched in Li, F, Rb, and Cs and depleted in Fe relative to cores (Table 4). This trend is taken to represent the compositional evolution occurring during the initial crystallization of the original Li-rich micas. In the final section we will discuss whether these phases formed by late stage magmatic or by sub-solidus processes.

S.W. England micas. Fig. 2 shows the relationship between average Li_2O (wt.%) and average SiO_2, Al_2O_3 and F (wt.%). The biotites and Li-rich micas define a clear positive correlation between SiO_2 and Li_2O for samples from both S.W. England and France (Fig. 2*a*); muscovites plot above this trend at the low-Li end. Conversely, muscovites and Li-rich micas from St Austell and Megiliggar define a negative correlation between Al_2O_3 and Li_2O (Fig. 2*b*) with the biotites plotting below this trend. Li-rich micas from Meldon and France tend to be more aluminous and plot in a parallel trend (Fig. 2*b*). Biotites, muscovites and Li-rich micas all show the same clear positive correlation between F and Li_2O (Fig. 2*c*). These trends have been used to estimate average Li_2O contents for micas from samples not analysed for Li (model Li_2O values are identified with double asterisks in Tables 1 and 2). The Li_2O values estimated for a particular sample based on average SiO_2, Al_2O_3 and F contents show very close agreement ($\pm$5% relative).

A general review of the data in Table 1 shows that the most Li-rich micas tend to have generally higher Si, F, Rb and Cs and lower Al and Fe contents. Octahedral site occupancy is usually close to 6 atoms while the 12-co-ordinated sites show variable deficiencies even in samples ana-

Table 1 Average analyses for micas in granitic rocks from S.W. England.

	Biotite granite				Megacrystic Li-mica granites					Non-megacrystic Li-mica granites	
	5007 (Bi)	5007 (Musc)	5089 (Bi)	5089 (Musc)	5093	5024	5011	5106	5096	5001	5020
No. anals.+	(9)	(3)	(13)	(5)	(9)	(12)	(9)	(19)	(8)	(9)	(20)
Ident. no.++	1	1	8	8	9	10	7	6	5	2	4
SiO_2	36.17(.46)¤	45.89(.70)	37.00(.47)	46.22(.49)	48.08(1.8)	44.77(.59)	47.59(.97)	41.51(1.1)	45.21(1.3)	49.40(1.5)	48.78(1.8)
TiO_2	2.48(.40)	0.41(.30)	2.58(.14)	0.36(.15)	0.15(.17)	0.32(.16)	0.21(.14)	0.79(.15)	0.44(.21)	0.16(.16)	0.24(.13)
Al_2O_3	20.58(.43)	33.44(.01)	20.76(.14)	34.05(.72)	20.33(1.1)	21.89(.80)	20.47(.79)	24.50(.60)	27.56(1.3)	20.52(.89)	19.86(.85)
FeO*	20.87(.65)	1.98(.14)	20.63(.35)	1.91(.27)	9.11(.74)	11.72(.88)	7.80(.78)	11.70(.91)	8.30(1.6)	7.60(.86)	6.43(.55)
MnO	0.41(.18)	n.d.	0.37(.14)	0.10(.09)	0.58(.07)	n.a.	0.59(.14)	0.49(.16)	0.14(.13)	0.68(.10)	0.56(.08)
MgO	4.87(.18)	1.26(.04)	4.68(.35)	0.94(.11)	n.d.	0.81(.12)	0.47(.10)	1.41(.14)	1.06(.23)	n.d.	n.d.
CaO	n.d.	n.d.	n.d.	n.d.	n.d.	n.d.	n.d.	n.d.	n.d.	n.d.	n.d.
Li_2O	1.64(.24)	0.39(.05)	1.71(.28)	0.11**	5.00(.50)	3.53(.66)	4.91(.54)	2.82(1.0)	1.71(.31)	5.50(.53)	5.1**
Na_2O	0.22(.25)	0.73(.04)	0.55(.22)	0.63(.19)	0.17(.19)	0.06(.07)	0.20(.22)	0.38(.14)	n.d.	0.44(.18)	0.26(.13)
K_2O	9.33(.12)	10.34(.28)	9.45(.15)	10.00(.16)	9.77(.30)	10.26(.17)	10.09(.18)	9.75(.26)	10.45(.17)	10.03(.16)	9.99(.18)
Rb_2O	n.a.	n.a.	0.28(.05)	n.a.	*0.84(.09)*	n.d.	n.d.	*0.64(.08)*	n.d.	*0.77(.18)*	*1.09(.11)*
Cs_2O	n.a.	n.a.	0.02(.02)	n.a.	0.26(.12)	n.d.	n.d.	0.12(.05)	n.d.	0.03(.02)	0.08(.06)
F	2.03(.16)	1.25(.05)	1.89(.15)	n.a.	6.94(.45)	6.33(.61)	7.03(.29)	4.40(.32)	3.86(.57)	6.62(.52)	6.82(.34)
Minus F≡O	0.86	0.53	0.80	-	2.92	2.66	2.96	1.85	1.63	2.79	2.87
Total	97.74	95.16	99.12	94.32	98.31	97.03	96.40	96.66	97.10	98.96	96.34
Cell formulae (to 22 oxygens)											
Si	5.413	6.188	5.455	6.220	6.727	6.419	6.715	5.995	6.273	6.786	6.873
Al^{IV}	2.587	1.812	2.545	1.780	1.273	1.581	1.285	2.005	1.727	1.224	1.127
Al^{VI}	1.045	3.547	1.063	3.622	2.081	2.119	2.120	2.167	2.781	2.094	2.172
Ti	0.279	0.042	0.286	0.036	0.015	0.035	0.022	0.086	0.046	0.017	0.025
Fe	2.613	0.223	2.544	0.215	1.067	1.405	0.920	1.413	0.963	0.872	0.758
Mn	0.052	-	0.046	0.011	-	0.071	0.060	0.060	0.079	0.067	0.067
Mg	1.087	0.253	1.028	0.189	-	0.173	0.099	0.303	0.219	-	-
Li	0.986	0.210	1.014	0.054	2.812	2.036	2.787	1.638	0.954	3.034	2.890
Total Y	6.062	4.233	5.981	4.127	6.044	5.768	6.019	5.667	4.979	6.096	5.912
Ca	-	-	-	-	-	-	-	-	-	-	-
Na	0.064	0.192	0.157	0.164	0.047	0.017	0.055	0.106	-	0.117	0.071
K	1.781	1.778	1.777	1.717	1.745	1.877	1.816	1.797	1.850	1.755	1.796
Rb	-	-	*0.027*	-	*0.076*	-	-	*0.059*	-	*0.068*	*0.099*
Cs	-	-	0.001	-	0.016	-	-	0.007	-	0.002	0.005
Total X	1.845	1.970	1.962	1.881	1.884	1.894	1.871	1.969	1.850	1.942	1.971
F	0.961	0.540	0.881	-	3.072	2.870	3.137	2.010	1.694	2.872	3.039
I.E.	0.71	0.47	0.72	0.54	1.0	0.89	0.91	0.83	0.82	1.0	1.0

+ Number of analyses spots in average; ++ Identification number used in Figs. 2, 3 and 4 (see appendix);
¤ Standard deviations in parentheses (1σ); * Total Fe as FeO; ** Li_2O estimated from SiO_2, Al_2O_3 and F contents (Fig. 2);
n.a. not analysed; n.d. not detected; Cl was below the detection limit (~0.06 wt%) in all micas;
I.E. = (Fe+Mn)/(Fe+Mn+Mg) (atomic).

Table 1 (Continued)

	Non-megacrystic Li-mica granites								Meldon aplite		Megiliggar aplite
	5015	5022	5031	5081	5005 (I)	5080	5085	5017	5016	5003	5100
No. anals.+	(15)	(4)	(10)	(8)	(11)	(5)	(4)	(13)	(7)	(9)	(14)
Ident. no.++	3	11	12	14	16	13	15	17	19	18	20
SiO_2	51.04(1.3)‡‡	47.46(.63)	47.62(1.8)	46.26(1.4)	48.30(1.1)	48.64(.68)	46.02(.34)	47.28(.43)	46.23(2.1)	47.69(1.9)	48.53(1.5)
TiO_2	0.10(.10)	0.35(.02)	0.22(.17)	0.42(.18)	0.27(.20)	0.20(.13)	0.14(.10)	0.29(.11)	0.25(.14)	0.28(.20)	0.20(.17)
Al_2O_3	20.60(.85)	20.53(.39)	20.48(1.0)	21.60(.59)	20.39(.79)	31.01(.82)	35.94(1.9)	35.03(.94)	23.85(2.1)	25.27(2.1)	21.09(.96)
FeO*	5.85(.81)	10.53(.53)	11.58(1.5)	11.17(.87)	9.91(.83)	4.28(.86)	0.38(.55)	0.46(.27)	3.64(.23)	3.98(.82)	8.67(.79)
MnO	0.63(.11)	0.09(.18)	n.a.	0.20(.17)	0.11(.10)	n.d.	n.d.	n.d.	1.07(.15)	0.89(.22)	0.99(.29)
MgO	0.81(.12)	n.d.	n.d.	n.d.	0.89(.29)	n.d.	0.17(.33)	0.80(.24)	n.d.	n.d.	n.d.
CaO	0.10(.05)	n.d.	n.d.	n.d.	0.03(.03)	n.d.	n.d.	n.d.	0.06(.07)	n.d.	n.d.
Li_2O	5.78(.33)	4.5**	3.73(.80)	4.0**	4.04(.48)	0.9**	0.2**	0.02	5.10(.49)	3.99(1.1)	4.86(.81)
Na_2O	0.59(.15)	0.08(.16)	0.03(.04)	0.23(.19)	0.46(.13)	n.d.	0.22(.15)	0.28(.13)	0.38(.04)	0.28(.21)	0.22(.19)
K_2O	9.83(.16)	9.97(.25)	9.88(.28)	9.93(.20)	9.80(.48)	10.06(.52)	10.29(.28)	10.55(.26)	10.44(.15)	10.52(.25)	9.84(.12)
Rb_2O	n.a.	0.94(.07)	n.a.	1.06(.08)	n.a.	0.21(.06)	0.17(.09)	n.a.	0.89(.19)	n.a.	n.a.
Cs_2O	n.a.	0.08(.04)	n.a.	0.10(.02)	n.a.	0.03(.01)	n.d.	n.a.	0.02(.01)	n.a.	n.a.
F	8.73(.36)	6.34(.11)	5.23(.58)	6.04(.32)	8.21(.82)	1.98(.35)	1.01(.34)	0.15	6.67(1.5)	6.38(.99)	6.85(.65)
Minus F=O	3.68	2.67	2.20	2.54	3.46	0.83	0.43	0.06	2.81	2.69	2.88
Total	100.38	98.20	96.58	98.47	98.95	96.48	94.11	94.80	95.79	96.59	98.37
Cell formulae (to 22 oxygens)											
Si	6.852	6.674	6.746	6.531	6.741	6.513	6.188	5.995	6.495	6.575	6.714
Al^{IV}	1.148	1.326	1.254	1.469	1.259	1.487	1.812	2.005	1.505	1.425	1.286
Al^{VI}	2.113	2.078	2.166	2.126	2.096	3.408	3.885	3.773	2.445	2.682	2.154
Ti	0.010	0.037	0.023	0.045	0.028	0.020	0.014	0.029	0.026	0.029	0.021
Fe	0.657	1.237	1.372	1.319	1.157	0.479	0.043	0.051	0.428	0.459	1.003
Mn	0.072	0.011	-	0.024	0.013	-	-	-	0.127	0.104	0.116
Mg	0.162	-	-	-	0.185	-	0.034	0.158	-	-	-
Li	3.121	2.545	2.125	2.272	2.268	0.485	0.108	0.011	2.882	2.213	2.705
Total Y	6.135	5.909	5.686	5.786	5.747	4.392	4.084	4.022	5.911	5.487	5.999
Ca	0.014	-	-	-	0.004	-	-	-	0.009	-	-
Na	0.154	0.022	0.008	0.063	0.124	-	0.057	0.072	0.104	0.075	0.059
K	1.684	1.789	1.786	1.789	1.745	1.719	1.765	1.789	1.871	1.850	1.737
Rb	-	0.085	-	0.096	-	0.018	0.015	-	0.080	-	-
Cs	-	0.005	-	0.006	-	0.002	-	-	0.001	-	-
Total X	1.852	1.896	1.794	1.954	1.873	1.737	1.837	1.861	2.065	1.925	1.796
F	3.707	2.820	2.343	2.697	3.624	0.838	0.430	0.066	2.963	2.782	2.997
I.E.	0.82	1.0	1.0	1.0	0.86	1.0	0.56	0.24	1.0	1.0	1.0

+ Number of analyses spots in average; ++ Identification number used in Figs. 2, 3 and 4 (see appendix);
‡‡ Standard deviations in parentheses (1σ); * Total Fe as FeO; ** Li_2O estimated from SiO_2, Al_2O_3 and F contents (Fig. 2);
n.a. not analysed; n.d. not detected; Cl was below the detection limit (~0.06 wt.%) in all micas;
I.E. = (Fe+Mn)/(Fe+Mn+Mg) (atomic).

Table 2 Average analyses for altered mica populations coexisting with less-altered Li-micas.

	Megacrystic Li-mica granite		Non-megacrystic Li-mica granites			
	5011	5106	5081	5005 (IV)	5005 (II)	5005 (III)
No. anals.	(2)	(3)	(3)	(2)	(3)	(4)
Ident. no.	7	6	14	16	16	16
SiO_2	43.76(.56)	43.92(1.7)	47.73(1.6)	45.70(1.1)	46.55(.97)	46.52(.46)
TiO_2	0.54(.10)	0.59(.22)	0.25(.22)	0.20(.03)	0.37(.01)	0.26(.08)
Al_2O_3	28.17(.30)	27.08(2.5)	30.00(1.2)	30.97(.88)	22.13(1.5)	31.13(.94)
FeO*	7.00(.76)	7.42(2.0)	4.57(1.7)	4.31(.65)	10.29(1.2)	4.02(.89)
MnO	0.35(.04)	0.31(.27)	0.07(.06)	0.04(.05)	0.15(.04)	0.03(.03)
MgO	0.54(.28)	1.12(.21)	0.22(.30)	1.49(.01)	1.27(.26)	0.95(.19)
CaO	n.d.	n.d.	n.d.	0.12(.02)	0.07(.08)	n.d.
Li_2O	3.75(.72)	2.52(.22)	1.1**	0.61(.16)	0.88(.42)	3.06(.46)
Na_2O	0.52(.09)	n.d.	n.d.	0.48(.19)	0.55(.12)	0.58(.20)
K_2O	10.47(.20)	9.76(.58)	10.05(.97)	10.24(.09)	10.37(.42)	9.97(.25)
Rb_2O	n.d.	n.a.	0.30(.18)	n.a.	n.a.	n.a.
Cs_2O	n.a.	n.a.	0.02(.02)	n.a.	n.a.	n.a.
F	5.03(1.9)	3.27(.69)	2.21(.88)	1.90(.26)	6.28(1.2)	2.23(.47)
Minus F=O	2.12	1.38	0.93	0.80	2.65	0.94
Total	98.01	94.61	95.59	95.22	96.26	97.81
Cell formulae (to 22 oxygens)						
Si	6.023	6.192	6.489	6.257	6.719	6.152
Al^{IV}	1.977	1.808	1.511	1.743	1.281	1.848
Al^{VI}	2.594	2.693	3.297	3.256	2.485	3.005
Ti	0.056	0.063	0.026	0.021	0.040	0.026
Fe	0.806	0.875	0.520	0.494	1.242	0.445
Mn	0.041	0.037	0.008	0.005	0.018	0.003
Mg	0.111	0.235	0.045	0.304	0.273	0.187
Li	2.076	1.429	0.602	0.336	0.511	1.628
Total Y	5.684	5.332	4.498	4.416	4.569	5.294
Ca	-	-	-	0.018	0.011	-
Na	0.139	-	-	0.127	0.154	0.149
K	1.839	1.755	1.743	1.789	1.910	1.682
Rb	-	-	0.026	-	-	-
Cs	-	-	0.001	-	-	-
Total X	1.978	1.755	1.770	1.934	2.075	1.831
F	2.190	1.458	0.950	0.823	2.867	0.933
I.E.	0.88	0.80	0.92	0.62	0.82	0.71

lysed for Rb and Cs. The more altered micas (Table 2) tend to have low Li, Rb and Cs, particularly high Al contents and, as a consequence, lower octahedral site totals.

The average analyses of the micas reported in Tables 1 and 3 (least-altered types in each rock) are plotted in Fig. 3; this figure is slightly different from the Foster (1960) variation diagram in that all Fe is plotted as Fe^{2+}. The Fe-rich micas in BG 5007 (point 1 in Fig. 3) and in BG 5089 from within the MLG unit (Goonbarrow; point 8) are compositionally very similar and can be classified as siderophyllites (after Stone *et al.*, 1988). The Fe-poor micas (muscovites) from BG 5007 and 5089 are also compositionally similar. This, together with petrographic similarities, suggests that the biotite granite exposed in Goonbarrow may be part of the nearby main biotite granite mass (Fig. 1), perhaps connected at depth. The siderophyllite compositions in 5007 and 5089 are very similar to the ion/electron-microprobe analysis of mica from a nearby locality (Wilson and Long, 1983). In comparison with chemically analysed siderophyllites from other localities in the S.W. England granite batholith, the present data show that the micas are richer in Li and F than mica from Dartmoor (Al-Saleh *et al.*, 1977), more magnesian and less F-rich than mica from Cligga Head (Hall, 1971), and within the compositional range for micas from type-B granites from the Lands End, Carnmenellis, and Scilly Isles intrusions (Stone *et al.*, 1988) except for its slightly higher Li content (1.6% Li_2O compared with a range of 0.6–1.0%). The Fe-poor micas from 5007 and 5089 are slightly more aluminous and less Fe- and F-rich than muscovites from unaltered Cligga Head granite (Hall, 1971). Muscovites from biotite granites are poorer in Li and F than coexisting siderophyllites; this relationship is the same as for coexisting micas in the Cligga Head granite (Hall, 1971).

All the MLG studied contain a single original mica which is invariably Li-rich. The unaltered Li-rich micas in the St Austell MLG show a substantial increase in Li accompanied by a decrease in R^{2+} with much less variation in (Al + Ti) (Fig. 3). Micas from 5096 (point 5, Fig. 3), 5106 (6), and 5024 (10) are zinnwaldites while those from 5011 (7) and 5093 (9) are lepidolites. Mica from 5096 (5) is less Li-rich and rather more aluminous than the others and it should be noted that this rock is the most altered MLG studied (see later). In the MLG unit the Li-rich micas have values for an iron enrichment (*IE*) index [(ΣFe + Mn)/

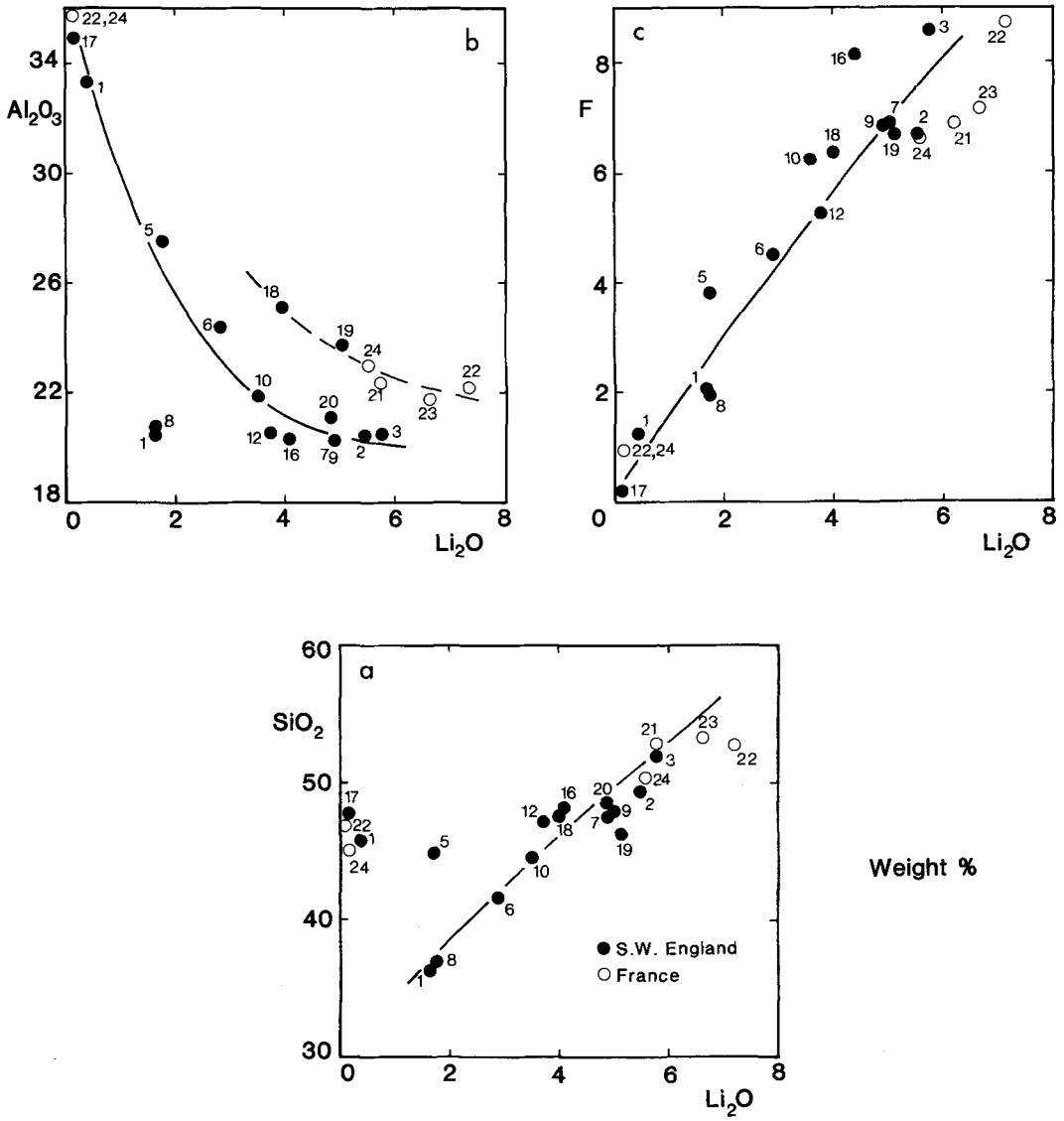

FIG. 2. Plots of averaged microprobe data (Tables 1 and 3) for SiO_2 (Fig. 2*a*), Al_2O_3 (2*b*), and F (2*c*) *vs.* Li_2O (wt.%); curves are drawn by eye. Note that in Fig. 2*b* the Fe-poor lepidolites are displaced to higher Al contents relative to the normal trend. These curves have been used to estimate Li_2O for some samples not analysed by ion microprobe. Numbered points are identified in Tables 1 and 3 and in the Appendix.

(ΣFe + Mn + Mg), atomic] varying from 0.72 to 1.0 (Table 1). The less Li-rich types have the lowest *IE* ratios as well as the highest Ti and lowest F, Rb, and Cs contents; thus the order of evolution is deduced to be 5106 (5096?) → 5024 → 5011, 5093.

The non-megacrystic Li-mica granites (NMLG) all contain a single original mica. The compositional range for unaltered mica is slightly more restricted than in the MLG but the most Li-rich types have higher Li than their equivalents in the MLG (Table 1, Fig. 3). Increasing Li is again accompanied by decreasing R^{2+} and little change in (Al + Ti). Micas from 5031 (12), 5005 (16), 5081 (14)

Table 3 Average analyses of micas from French granites.

	Beauvoir				Montebras	
	5050	5052	5052(Musc)	5054	5062	5062(Musc)
No. anals.	(8)	(8)	(5)	(9)	(6)	(7)
Ident. no.	21	22	22	23	24	24
SiO_2	52.90(.59)	53.01(.47)	46.83 (.90)	53.47(.81)	50.37(.71)	44.98(.76)
TiO_2	n.d.	n.d.	n.d.	n.d.	n.d.	n.d.
Al_2O_3	22.44(.53)	22.35(.65)	36.63(.64)	21.81(.68)	23.11(1.8)	36.01(.32)
FeO*	0.21(.23)	0.04(.05)	0.22(.14)	0.39(.07)	2.47(.49)	0.37(.26)
MnO	n.d.	0.20(.21)	0.12(.07)	0.14(.11)	1.08(.21)	n.d
MgO	n.d.	n.d.	0.24(.19)	n.d.	n.d.	n.d.
CaO	n.d.	n.d.	n.d.	n.d.	n.d.	n.d.
Li_2O	5.77(.66)	7.41(.49)	n.d.	6.65(.95)	5.58(.78)	0.10(.07)
Na_2O	0.41(.25)	0.42(.28)	0.14(.14)	0.42(.11)	0.32(.17)	n.d.
K_2O	9.84(.21)	9.89(.14)	9.30(.29)	9.87(.32)	9.64(.17)	10.54(.53)
Rb_2O	n.a.	n.a.	n.a.	1.17(.27)	n.a.	n.a.
Cs_2O	n.a.	n.a.	n.a.	0.13(.16)	n.a.	n.a.
F	7.14(.28)	8.81(.29)	n.a.	6.82(.26)	6.56(.96)	1.15(.56)
Minus F=O	3.01	3.71	-	2.87	2.76	0.48
Total	95.70	98.42	93.48	98.00	96.37	92.67
Cell formulae (to 22 oxygens)						
Si	7.099	6.974	6.238	7.068	6.829	6.151
Al^{IV}	0.901	1.026	1.762	0.932	1.171	1.849
Al^{VI}	2.649	2.441	3.991	2.467	2.523	3.957
Ti	-	-	-	-	-	-
Fe	0.024	0.004	0.025	0.043	0.280	0.042
Mn	-	-	0.014	0.016	0.124	-
Mg	-	-	0.048	-	-	-
Li	3.115	3.921	-	3.536	3.043	0.055
Total Y	5.788	6.368	4.078	6.062	5.970	4.054
Ca	-	-	-	-	-	-
Na	0.107	0.107	0.036	0.108	0.084	-
K	1.685	1.660	1.581	1.664	1.667	1.839
Rb	-	-	-	0.099	-	-
Cs	-	-	-	0.007	-	-
Total X	1.792	1.767	1.617	1.878	1.751	1.839
F	3.030	3.666	-	2.851	2.813	0.497
I.E.	1.0	1.0	0.59	1.0	1.0	1.0

and 5022 (11) are zinnwaldites while those from 5001 (2), 5020 (4) and 5015 (3) are more evolved and are lepidolites. The lepidolites tend to be more F-rich than the zinnwaldites while both have *IE* close to 1.0. The NMLG containing lepidolites are all from Gunheath supporting the suggestion (Manning, 1988) that the Hensbarrow stock is a more evolved part (roof zone) of a differentiated topaz granite (NMLG) body with the Nanpean stock representing a deeper level. In the progressively more altered NMLG rocks the original micas are substantially recrystallized with Al becoming enriched and Li, Fe, F, Rb, and Cs becoming depleted (5080 → 5085 → 5017) (cf. alteration trends reported by Hall, 1971, and Manning and Exley, 1984).

The inter-sample trend for the unaltered micas in the BG, MLG and NMLG is shown by the arrow labelled 'original' in Fig. 3. This trend shows that the overall variation is an increase in Li combined with a decrease in R^{2+} and a small increase in (Al + Ti). Alteration of the original micas can be represented by vectors towards the Al apex and one such trend is shown by the arrow labelled 'altered' in Fig. 3. The inter-sample alteration trends identified for both the MLG and NMLG can also be seen within single samples for both rock units. Thus, for MLG samples 5011 and 5106 two mica compositional populations can be identified (cf. Tables 1 and 2); one represents the original (unaltered) micas and the other the altered micas. Within the NMLG, 5081 also shows two populations while 5005 is even more complex with four compositional groups (Tables 1 and 2). Analysis group 5005(II) is somewhat atypical in that the Li content is anomalously low for its Al, Fe and F contents. These compositional trends will be considered further using single spot analytical data.

Two samples of the Meldon aplite have been studied (5003 and 5016), both have lepidolites as the original micas (Fig. 3) in agreement with the chemical study of Chaudhry and Howie (1973*a*). The lower Li content of 5003 (point 18, Fig. 3) mica compared to 5016 (19) may be related to the generally more altered nature of the former rock. The mica from Megiliggar Rocks (sample 5100 (20)) is on the boundary between zinnwaldite and lepidolite.

French micas. Average analyses are given in Table 3 and are plotted in Fig. 3. All the Li micas are lepidolites (cf. Aubert, 1969; Levillain, 1981)

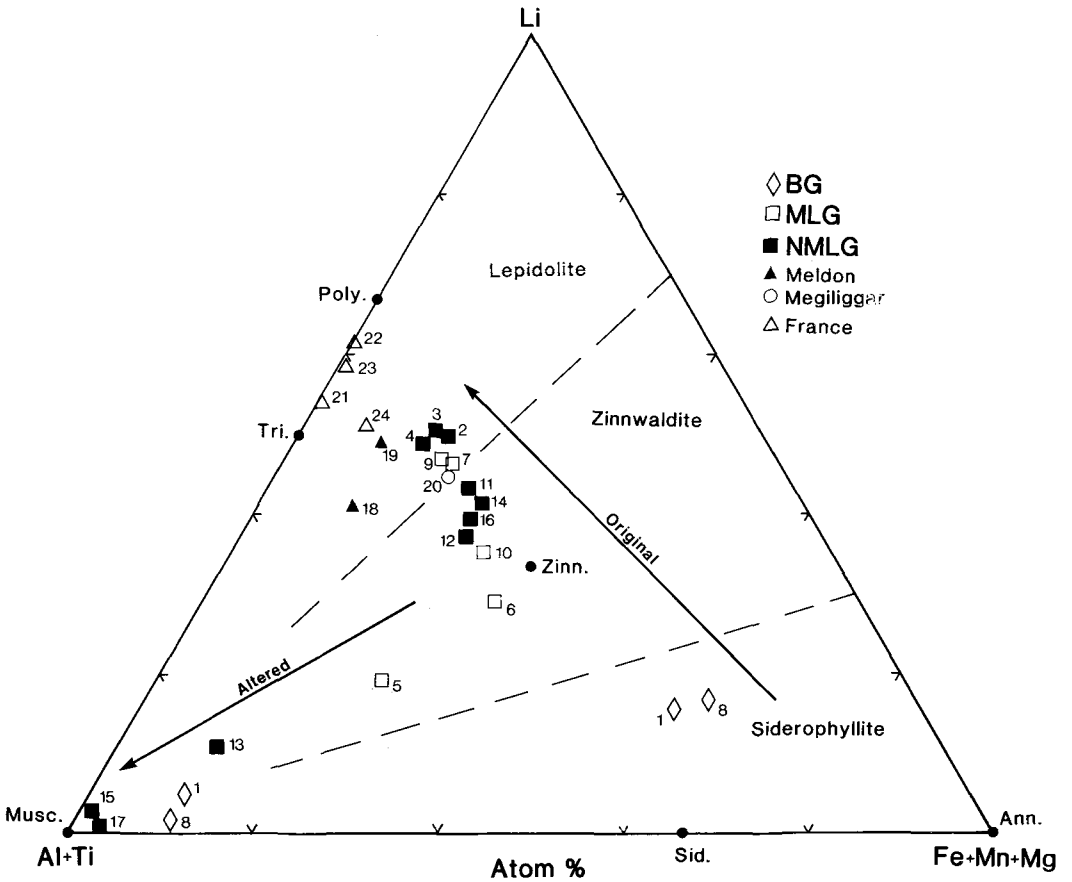

FIG. 3. Li–(Al + Ti)–[ΣFe (as Fe^{2+}) + Mn + Mg] octahedral site occupancy plot (atomic) for averaged microprobe data of the least-altered samples (Tables 1 and 3). Sample numbers are identified in Tables 1 and 3 and in the Appendix. Trends are shown for unaltered and altered micas. Abbreviations: Poly. = polylithionite; Tri. = trilithionite; Zinn. = zinnwaldite; Musc. = muscovite; Sid. = siderophyllite; Ann. = annite. Boundaries demarcating fields of lepidolite, zinnwaldite and siderophyllite are from Stone *et al.* (1988).

with those from Beauvoir being virtually Fe-free. These Beauvoir micas [5050 (point 21 in Fig. 3), 5052 (22), 5054 (23)] appear to have recrystallized from feldspars altered to Li-poor muscovite (cf. lepidolite and muscovite analyses for 5052 in Table 3) suggesting a sub-solidus origin involving very late stage Li metasomatism. By contrast the sample from Montebras [5062 (24)] is much less altered and the Li-rich mica appears to have primary textures. Hydrothermal alteration of this primary low-Fe mica has produced secondary muscovite similar to that in the Beauvoir granites (Table 3).

Compositional and element substitution trends. In the Fe-bearing Li-mica series the substitution mechanism for the siderophyllite → zinnwaldite → polylithionite series (ideal formulae) can be summarized:

$$Li^{VI} + Si^{IV} = (Fe^{2+})^{VI} + Al^{IV} \quad (1)$$

In this substitution, octahedral site occupancy is maintained at 6.0 atoms. According to this substitution Li replaces R^{2+} in the octahedral sites on a 1:1 basis and octahedral Al is not involved.

In the aluminous Li-mica muscovite → trilithionite series the substitution is:

$$3Li^{VI} = Al^{VI} + 2\square^{VI} \text{ (where } \square = \text{a vacancy)} \quad (2)$$

while that in the muscovite → polylithionite series would be:

$$4Li^{VI} + 2Si^{IV} = 2Al^{VI} + 2\square^{VI} + 2Al^{IV} \quad (3)$$

For chemical analyses of mica separated from the Meldon aplite, Chaudhry and Howie (1973*a*) found Li:Al^{VI} ratios varying between 3 and 2; this indicates that both substitutions (2) and (3) were operative (cf. Foster, 1960). Stone *et al.* (1988) concluded that Fe-rich micas from S.W. England show essentially continuous variation from siderophyllite through zinnwaldite to lepidolite. The variation was believed to be due principally to Li–R^{2+} substitution accompanied by a slight increase in octahedral R^{3+} (mainly Al). This trend appears to be well demonstrated by octahedral R^{3+}–R^{2+}–Li and 'Rieder (1970)-type' variation diagrams (see Stone *et al.*, 1988, Figs 3 and 4). The present data also seem to be generally consistent with this trend as can be seen from the arrow labelled 'original' in Fig. 3. However, these diagrams only take account of octahedral site occupancy without considering the coupled substitutions which may be necessary in other sites, e.g. Al → Si in 4-co-ordination.

The coupled effects of substitution in both octahedral and tetrahedral sites can be deduced from the vector diagrams of Černý and Burt (1984). Their plot for trioctahedral micas ($\square^{VI} = 0$) is particularly useful here. Fig. 4 shows the average analyses (Table 1) in this vector diagram, only those with the sum of octahedral cations between 5.7 and 6.1 being included. However, this data set includes all the unaltered micas from S.W. England except sample 5003 from Meldon. It seems that the main trend is from a hypothetical end-member between annite and siderophyllite, rather than from siderophyllite *sensu stricto*, towards polylithionite. The inter-sample trend shown by the present data can be approximated by the averaged formula:

$$2.2\,Li + 1.45\,Si = 0.66\,Al + 3R^{2+} \qquad (4)$$

This formula can be modified by allocation of Al to both tetrahedral and octahedral sites (assuming no octahedral vacancies):

$$2.2\,Li^{VI} + 0.79\,Al^{VI} + 1.45\,Si^{IV} = (3R^{2+})^{VI} + 1.45\,Al^{IV} \qquad (5)$$

This relationship for inter-sample variation is consistent with that reported by Stone *et al.* (1988). However, when the intra-sample microprobe compositional relations are considered the mechanisms are seen to be rather different.

Fig. 5 shows the relationship between Li and octahedral Al for the ion/electron-probe data (n.b. adjacent analyses are averaged or omitted on the figures to preserve clarity). Micas from BG 5007 and 5089 show little variation and are indistinguishable (Fig. 5*a*). MLG 5106 (Fig. 5*e*) shows the greatest range in composition and with a few exceptions the spot analyses show a negative correlation between Li and Al. The same type of correlation is also well shown for MLG 5093 (Fig. 5*b*), 5011 and 5024 (Fig. 5*f*). For each sample the Li:Al variation is close to a ratio of 3:1. The data for MLG 5096 (Fig. 5*b*) are more scattered reflecting the advanced alteration effects shown by this sample.

NMLG samples 5001, 5015 and 5031 (Fig. 5*c* and *g*) show similar trends while 5005 exhibits four populations of spot analyses, those labelled II, III and IV represent variously altered compositions with I being the least altered. Apart from the altered minerals the intra-sample Li:Al ratios seem to be close to, or greater than, 3:1. The displacement of altered micas to more Al-rich compositions has already been commented upon.

The mica trends for the Meldon aplite, Megiliggar Rocks and French samples also show the intra-sample Li:Al variation of 3:1.

Irrespective of whether they are zinnwaldites or lepidolites the S.W. England micas all show the Li:Al 3:1 variation and this is believed to represent the original intra-sample trends for the S.W. England samples at least. Thus the substitution mechanism (2) is clearly operative. This substitution is inevitably accompanied by an increase in the octahedral site occupancy with some samples showing rather little other chemical change (e.g. Table 4, MLG 5093 and NMLG 5005). However, in another sample (MLG 5106) the Li = Al substitution is accompanied by a decrease in Si (Table 4) indicating that other substitutions are occurring. The indication that the Li:Al ratio in the NMLG is greater than 3:1 suggests that the extra Li is accommodated by a substitution similar to mechanism (1) i.e. not involving octahedral Al.

In Fig. 6 the relations between Fe (ΣFe as Fe^{2+}) and Li are shown. As before, micas from BG 5007 and 5089 plot together in a tight group (Fig. 6*a*). MLG samples 5011, 5093 and 5024 show little variation in Fe with increasing Li (Fig. 6*c*); 5106 shows a similar relationship although more scattered (Fig. 6*a*). The analyses of the most altered MLG sample (5096) plot randomly (Fig. 6*c*). In the NMLG unit individual samples show slight decreases in Fe as Li increases (Fig. 6*b*); this trend is better shown when the inter-sample trend is considered. This negative correlation could result from the effects of F–Fe avoidance (Rosenberg and Foit, 1977) as Li and F are positively correlated (Foster, 1960, and this paper). Sample 5005 populations II, III and IV plot in separate groups away from the other analyses (Fig. 6*b*). The Meldon and Megiliggar mica show no variation in Fe as Li increases (Fig. 6*d*).

Overall, the intra-sample Fe–Li trends show

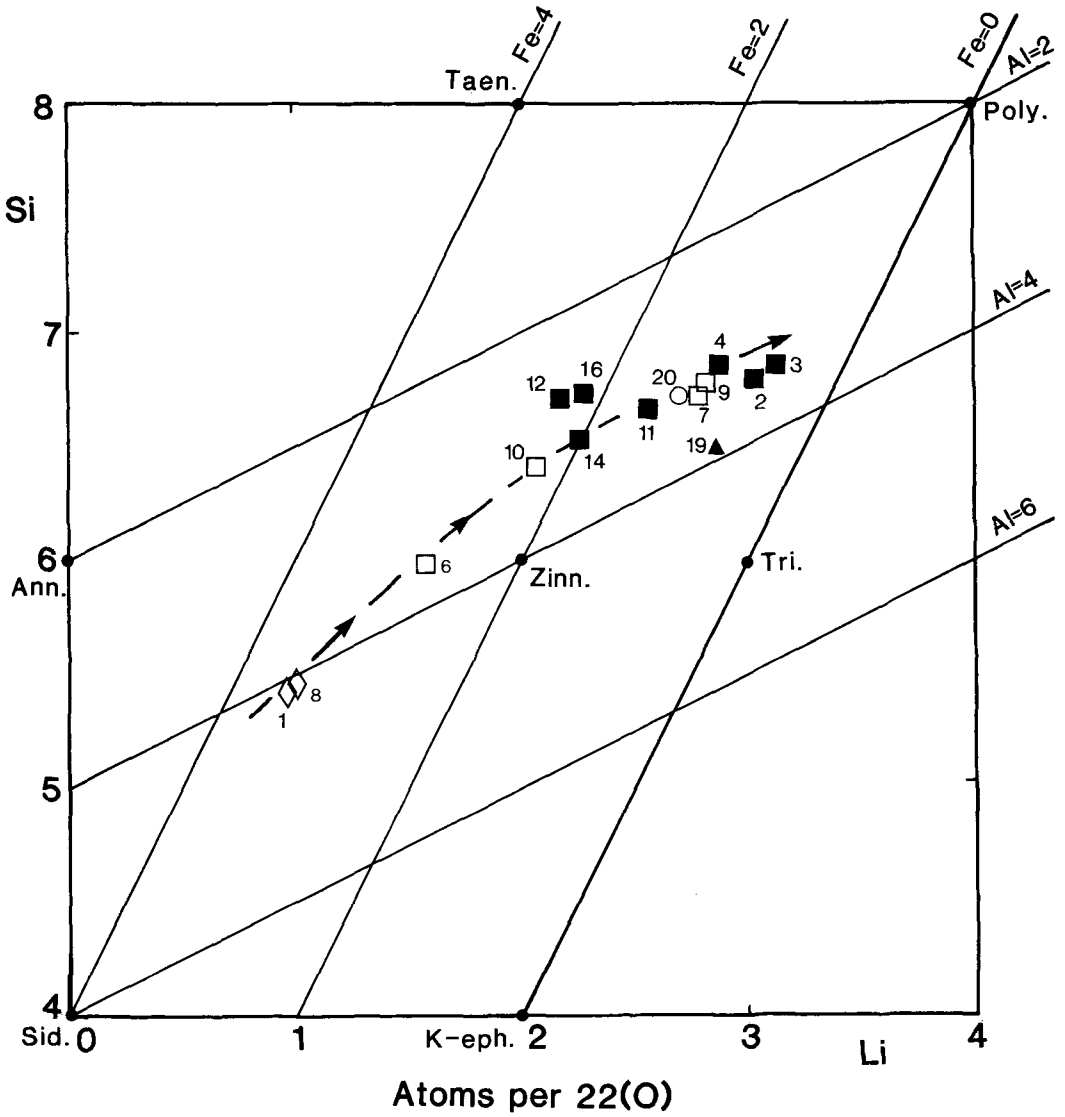

FIG. 4. Vector diagram (atomic) for averaged microprobe data. Note that the Al contents refer to the sum of octahedral and tetrahedral Al. The dashed trend is drawn by eye. Abbreviations as Fig. 3 plus: Taen. = taeniolite; K-eph. = K-ephesite.

that the Li = R^{2+} substitution is generally subordinate to the Li = Al substitution.

Li vs. F correlation. Foster (1960) and Rieder (1970) pointed out that Li-rich micas usually show a positive correlation between Li and F. Stone *et al.* (1988) and Monier and Robert (1986) confirmed this relationship for micas from S.W. England and the Massif Central, France, respectively. Average analyses for both original and altered micas from this study (Fig. 7*a*, Tables 1 and 2) also show a good correlation although one of the altered populations of MLG 5005 (II) shows anomalously high F for its Li content. Single spot analyses are also shown in Fig. 7*b–f* but intra-sample variations are generally rather scattered in each rock type. It is likely that both Li and F are particularly susceptible to local disturbance during incipient alteration and this is reflected for F by the common occurrence of fluorite along mica cleavage planes.

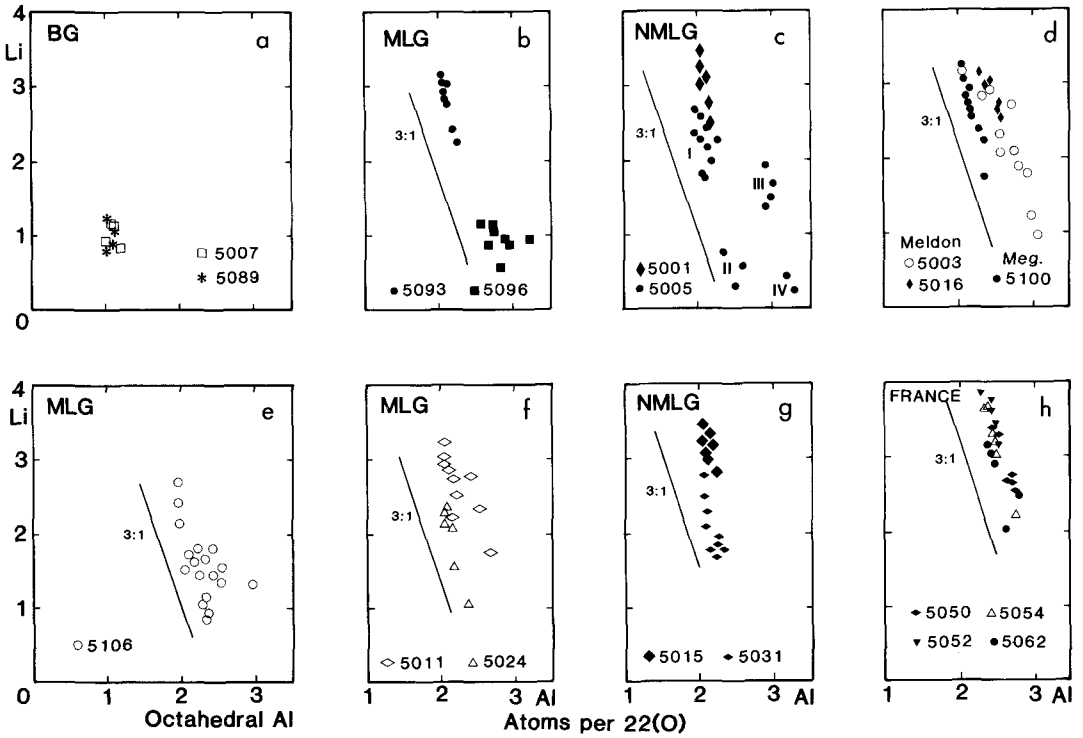

FIG. 5. Plots of Li *vs.* octahedral Al for microprobe spot analyses (atomic). Lines of slope Li:Al 3:1 are shown. Inter-sample trends either parallel the 3:1 lines or are slightly steeper. The trends for different samples are usually sub-parallel. Scattered points are due to various degrees of alteration. In Fig. 5*c* I–IV refer to different mica populations in 5005; I is the unaltered and II–IV the altered varieties.

Hydrothermal alteration indicators. It is clear from earlier discussion that Li-rich micas are particularly prone to sub-solidus recrystallization processes. Alteration is accompanied by progressive loss of Li, Fe, F, Rb and Cs, and enrichment in Al, eventually resulting in the formation of relatively F-poor muscovite (cf. Chaudhry and Howie, 1973*b*; Hall, 1971; Manning and Exley, 1984). In many of the diagrams discussed so far alteration effects produced significant amounts of scatter and, if ignored, would have made it difficult to identify the original trends.

In this work, plots of Fe against F have proved to be particularly valuable for identifying alteration trends (Fig. 8). Rosenberg and Foit (1977) pointed out that Fe and F tend to be negatively correlated in both micas and amphiboles and accounted for this using crystal field theory. In Fig. 8*b* both the inter- and intra-sample variations for BG 5007 and 5089 and MLG 5024, 5011 (except for 2 analyses), and 5093 show this antipathetic relationship clearly; some of the analyses for 5106 also plot on this trend. This negative F–Fe correlation is believed to be an original feature of these micas as the rocks defining it are the least altered types. A few analyses from 5106, 2 from 5011, and all from 5096 show an unexpected, but well developed, positive correlation (Fig. 8*b*). Sample 5096 is the most altered of all the MLG studied; the positive trend is, therefore, interpreted as an alteration/recrystallization trend. The NMLG samples 5031, 5081 (except for 2 analyses), 5001, 5020, 5022, and 5015 also show the negative correlation between Fe and F (Fig. 8*a*) which is again believed to be an original feature of the micas. Two of the 5005 populations (III and IV) and analyses from 5080, 5081 (2 points) and 5085 show a positive correlation which again reflects their degree of alteration. The least altered micas from 5005 (population I) plot above the trend for the other NMLG samples; the reason for this is not clear but incipient alteration effects involving redistribution of F may be responsible.

Analyses for the Meldon aplite and Megiliggar Rocks samples show fairly constant Fe contents as F varies (Fig. 8*c*). The Fe contents of the Li-rich

Table 4 Representative microprobe single spot analyses of Li-rich micas.

	Megacrystic Li-mica granites							Non-megacrystic Li-mica granites				Meldon		Megiliggar		Beauvoir	
	5093		5106			5096		5001		5005		5003		5100		5052	
	R#	C										C	R				
SiO_2	48.33	47.16	38.85	40.04	42.60	45.00	46.18	47.59	48.77	47.25	48.23	46.05	48.54	48.05	49.48	54.21	52.70
TiO_2	n.d.	n.d.	0.81	0.83	1.05	0.50	0.49	0.29	n.d.	0.25	0.35	0.44	0.44	0.44	n.d.	n.d.	n.d.
Al_2O_3	19.00	21.45	24.28	24.04	24.50	26.28	29.40	21.60	21.21	22.41	20.44	26.55	25.43	21.40	19.32	22.07	22.19
FeO*	8.19	9.92	13.45	14.00	11.84	10.72	6.40	8.20	7.66	10.35	9.78	3.81	3.51	8.87	7.62	0.42	0.49
MnO	0.56	0.64	0.58	0.69	0.54	n.d.	n.d.	0.75	0.67	0.20	0.02	0.91	0.80	1.33	1.08	0.19	n.d.
MgO	n.d.	n.d.	1.34	1.32	1.40	0.97	1.14	n.d.	n.d.	0.93	0.96	n.d.	n.d.	n.d.	n.d.	n.d.	n.d.
CaO	n.d.	n.d.	n.d.	n.d.	n.d.	n.d.	n.d.	n.d.	n.d.	n.d.	0.01	n.d.	n.d.	n.d.	n.d.	n.d.	n.d.
Li_2O	5.36	4.30	4.11	2.56	1.58	2.06	1.81	5.85	4.90	3.57	4.78	2.14	3.81	3.01	5.46	4.62	7.28
Na_2O	n.d.	n.d.	0.60	n.d.	n.d.	n.d.	n.d.	0.57	0.43	0.44	0.65	n.d.	n.d.	n.d.	n.d.	0.36	n.d.
K_2O	9.77	9.94	9.82	9.96	9.83	10.24	10.58	10.07	10.32	10.06	9.64	10.67	10.53	9.85	9.79	10.25	9.88
Rb_2O	0.88	0.91	0.75	0.55	n.a.	n.a.	n.a.	0.71	1.00	n.a.	n.a.	n.a.	n.a.	n.a.	n.a.	1.12	0.87
Cs_2O	0.32	0.11	0.16	0.05	n.a.	n.a.	n.a.	0.05	0.06	n.a.	n.a.	n.a.	n.a.	n.a.	n.a.	0.02	0.04
F	6.97	6.49	4.67	4.45	4.20	4.28	3.29	6.94	6.69	7.75	8.22	5.95	6.01	7.24	7.62	6.83	6.67
Minus F=O	2.93	2.73	1.97	1.88	1.77	1.80	1.39	2.93	2.82	3.27	3.46	2.51	2.53	3.05	3.21	2.88	2.81
Total	96.45	98.19	97.45	96.62	95.77	98.25	97.90	99.70	98.89	99.96	99.62	94.01	96.55	97.13	97.16	97.20	96.93
Cell formulae (to 22 oxygens)																	
Si	6.862	6.634	5.661	5.881	6.166	6.253	6.251	6.532	6.739	6.548	6.667	6.545	6.645	6.799	6.905	7.250	7.014
Al^{IV}	1.138	1.366	2.339	2.119	1.834	1.747	1.749	1.468	1.261	1.452	1.333	1.455	1.355	1.201	1.095	0.750	0.986
Al^{VI}	2.042	2.191	1.832	2.044	2.347	2.558	2.943	2.027	2.194	2.209	1.998	2.994	2.749	2.369	2.084	2.730	2.374
Ti	-	-	0.089	0.092	0.114	0.052	0.050	0.030	-	0.026	0.036	0.047	0.045	0.046	-	-	-
Fe	0.973	1.167	1.639	1.720	1.433	1.246	0.725	0.941	0.885	1.200	1.131	0.453	0.402	1.050	0.889	0.047	0.055
Mn	0.067	0.076	0.072	0.086	0.066	-	-	0.087	0.078	0.023	0.002	0.110	0.093	0.159	0.128	0.022	-
Mg	-	-	0.291	0.289	0.302	0.201	0.230	-	-	0.192	0.198	-	-	-	-	-	-
Li	3.061	2.433	2.409	1.512	0.920	1.151	0.985	3.230	2.724	1.990	2.658	1.223	2.098	1.713	3.065	2.485	3.897
Total Y	6.145	5.867	6.332	5.743	5.182	5.208	4.933	6.315	5.881	5.641	6.024	4.827	5.387	5.337	6.166	5.284	6.326
Ca	-	-	-	-	-	-	-	-	-	-	0.001	-	-	-	-	-	-
Na	-	-	0.170	-	-	-	-	0.152	0.115	0.118	0.174	-	-	-	-	0.093	0.103
K	1.770	1.784	1.826	1.866	1.815	1.815	1.827	1.763	1.819	1.779	1.700	1.935	1.839	1.778	1.743	1.749	1.678
Rb	0.080	0.082	0.070	0.052	-	-	-	0.063	0.089	-	-	-	-	-	-	0.096	0.074
Cs	0.019	0.007	0.010	0.003	-	-	-	0.003	0.004	-	-	-	-	-	-	0.001	0.002
Total X	1.869	1.873	2.079	1.921	1.815	1.815	1.827	1.981	2.027	1.897	1.874	1.934	1.839	1.778	1.743	1.939	1.857
F	3.365	2.887	2.152	2.067	1.923	1.881	1.408	3.013	2.924	3.397	3.593	2.675	2.602	3.240	3.363	2.889	2.808
I.E.	1.0	1.0	0.85	0.86	0.56	0.86	0.76	1.0	1.0	0.86	0.85	1.0	1.0	1.0	1.0	1.0	1.0

Spot locations: R = rim; C = core.

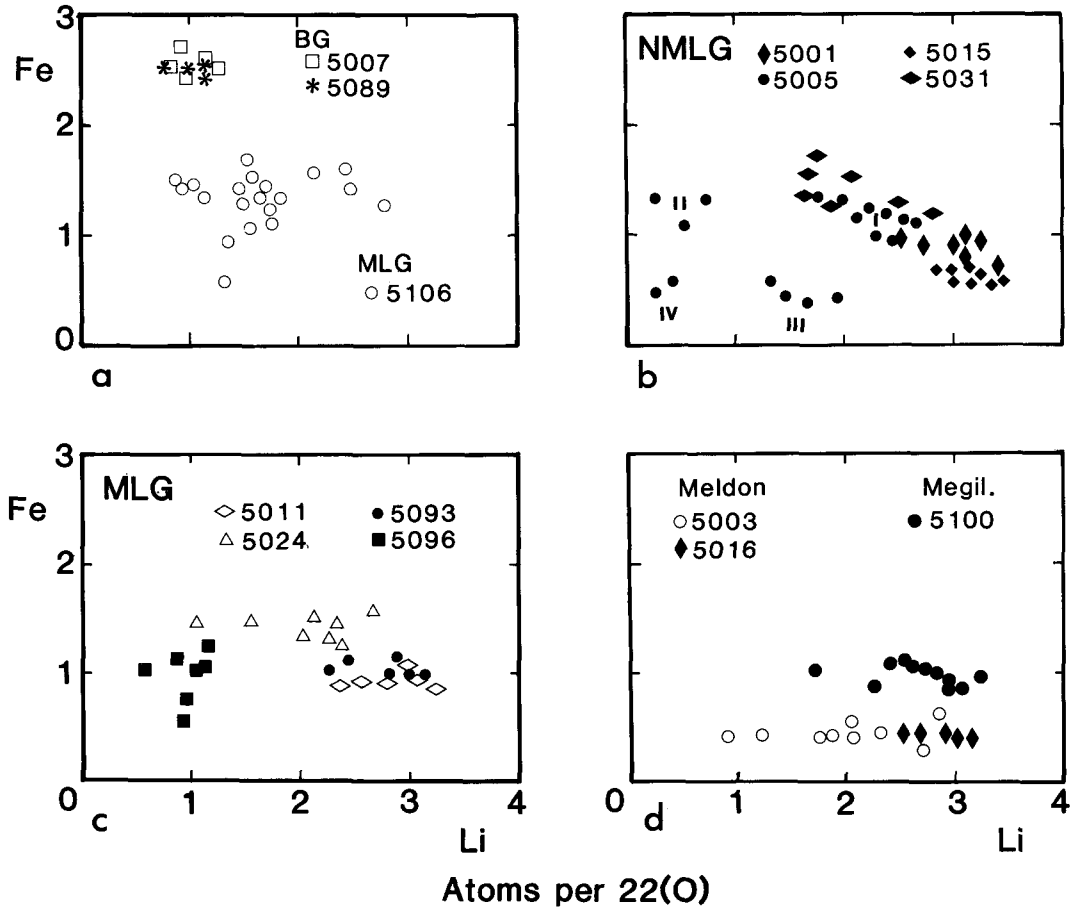

FIG. 6. Plot of Li *vs.* Fe (atomic) for microprobe spot analyses. Note that many samples show little inter-sample variation of Fe with increasing Li. In the NMLG, inter-sample variation shows decreasing Fe as Li increases and these trends for different samples overlap to define a steeper overall decreasing Fe trend.

micas from Montebras sample 5062 are too low to be sure of the trends but both the original mica and alteration trends are tentatively identified in Fig. 8*d*.

Microprobe spot analyses are plotted in the conventional Li–Al–R^{2+} diagram (Fig. 9). The original and alteration trends are shown on Fig. 9 to account for the displacement of some analyses towards the Al apex. The disposition of primary coexisting biotite and muscovite in the BG and of the Li-micas in MLG 5106 (Fig. 9*b*) confirm the form of the two mica solvus for Li-poor micas and its closure at higher Li contents (Monier and Robert, 1986). The original intra-sample trends for the MLG show that the main Li substitution mechanism is for Al rather than for R^{2+} i.e. trends are at low angles to lines of equal R^{2+} (lines C, D and E in Fig. 9). Note that the trends for the different samples are parallel rather than consecutive. The equivalent trends in the NMLG are slightly steeper but are again parallel (lines A and B in Fig. 9) suggesting that Li substitution for R^{2+} also occurs (cf. inverse Li–Fe relationship in Fig. 6*b*). However, the overall inter-sample trend (arrows labelled 'original' in Fig. 9) involves both substitutions to the same extent.

The differences between the intra-sample trends and the inter-sample trends for both the MLG and NMLG can be appreciated by comparing the slopes of the lines labelled A to E with those of the 'original' arrows in Fig. 9*a* and *b*. These different trends may reflect different scales of differentiation. Thus the overall ('original') trends may result from earlier, larger scale pro-

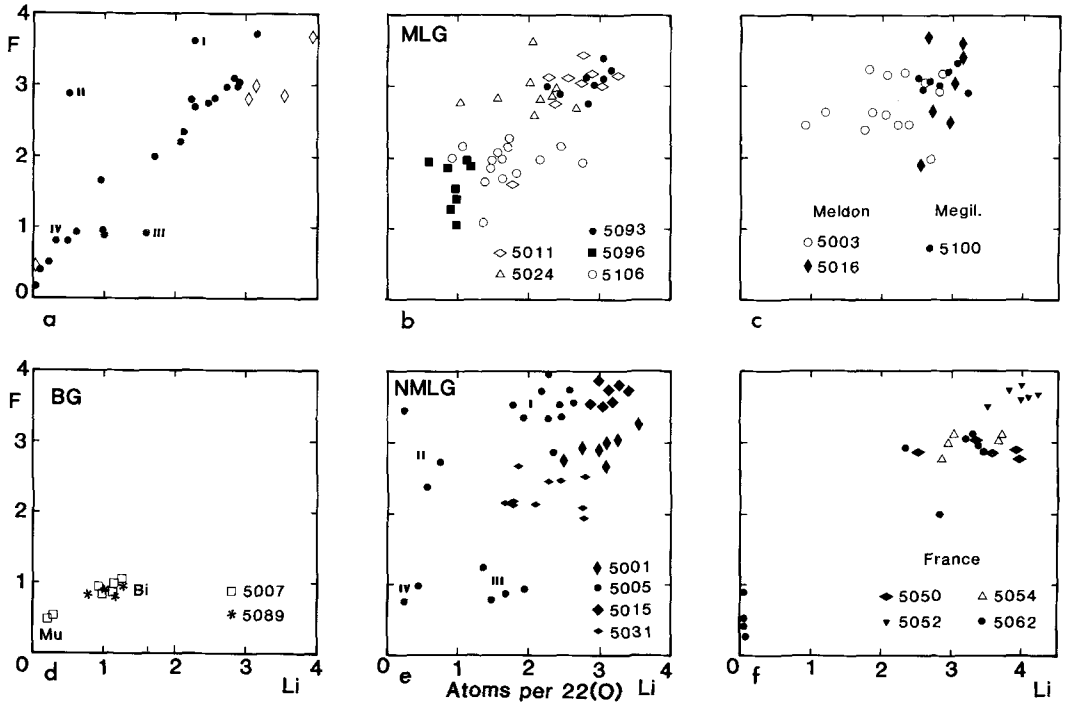

FIG. 7. Plot of Li *vs.* F (atomic) for microprobe spot analyses and for the average analyses. The positive Li–F relationship for the averaged data (Fig. 7*a*) is well defined but intra-sample variation is more scattered due to alteration effects.

cesses within the differentiating granite intrusion while the intra-sample trends reflect later, smaller scale processes involving late-stage growth of micas in the interstices of the feldspar–quartz grain assemblage.

Petrological significance

For the St Austell granite body petrographic and chemical information have been used to deduce an evolutionary series: biotite granite (BG) → megacrystic Li-mica granite (MLG) → non-megacrystic Li-mica granite (NMLG) → fluorite granite. There has been much discussion about the parts played by magmatic and metasomatic differentiation in forming this rock series. Exley (1959) suggested that magmatic differentiation was responsible while Stone (1975) believed that the BG had undergone alkali and volatile metasomatism to give rocks of Li-mica granite composition; Stone also suggested that these modified rocks may subsequently have been remelted to give late intruded bodies. Dangerfield *et al.* (1980) suggested that the MLG had been formed by metasomatism of BG with the metasomatizing fluids being derived from the NMLG. Based on an experimental study of the granite system in the presence of F, Manning (1982) postulated that the NMLG was a late-stage magmatic differentiate of the BG. He also suggested that the fluorite granite had formed by sub-solidus alteration of the NMLG and broadly agreed with Dangerfield *et al.* (1980) that the MLG was a metasomatic variant of the BG. Manning and Exley (1984) reinforced these ideas and set up models to account for the chemical changes in which the alkalis (including Li) and F released from the alteration of NMLG micas to form the fluorite granite pervasively penetrated the surrounding BG to form MLG. Thus they stressed the complementary relationship between the two supposedly altered rock types. Based on new mapping, Hill and Manning (1987) showed that the MLG unit was composed of several granite types including both magmatic and metasomatic varieties. The situation is clearly more complex than had been appreciated earlier.

The stage of formation of Li-rich micas in the magmatic rock types has also been discussed. Based on textural relations there is no doubt that

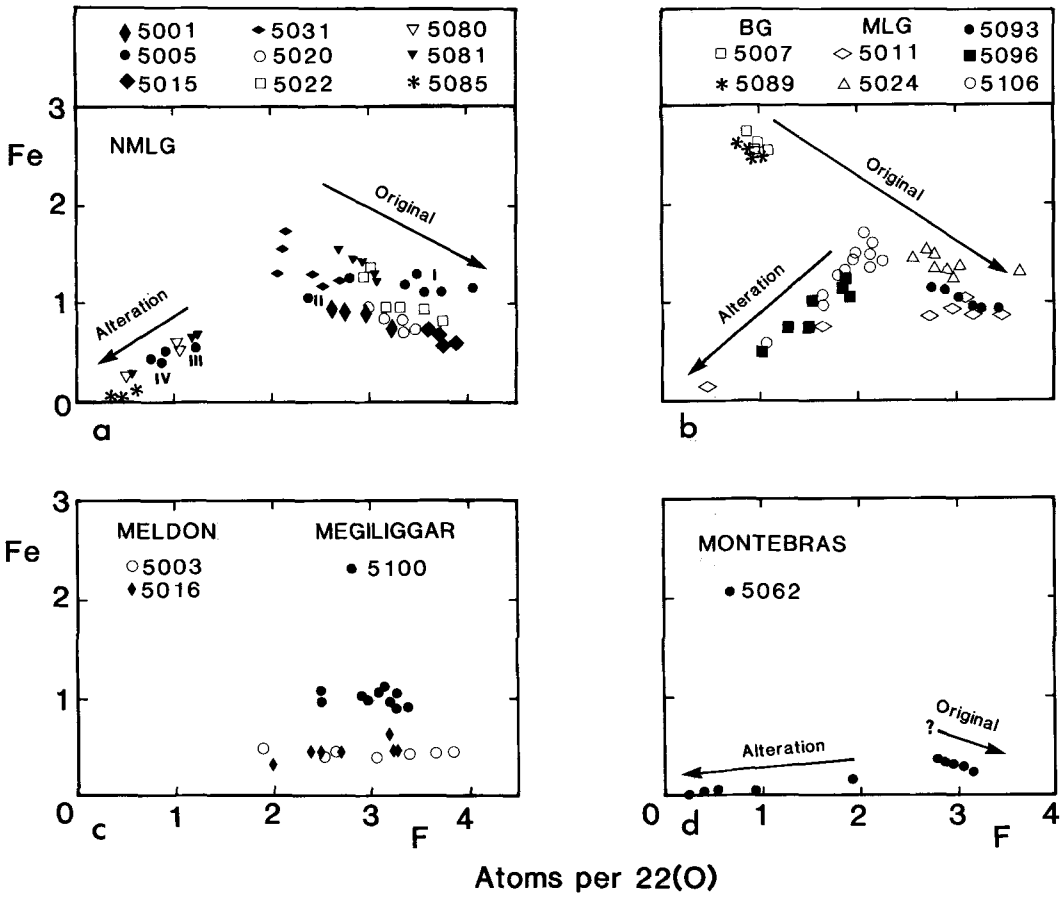

FIG. 8. Plot of Fe *vs.* F (atomic) for microprobe spot analyses. The trends for the unaltered (original) and altered samples are shown by arrows. The intra-sample original trends show decreasing Fe as F increases. These trends for different samples overlap to define a broader, steeper overall decreasing Fe trend.

they are late-crystallized phases but whether they formed during the final stages of magmatic differentiation (i.e. primary) or during sub-solidus recrystallization is less clear. Based on textural considerations, Stone (1975, 1984) and Stone *et al.* (1988) suggested that the zinnwaldites are all sub-solidus (secondary) but that the lepidolites from certain rock types (e.g. Tregonning leucogranites) could be late magmatic (primary).

In our discussion we will firstly consider whether Li-micas could be primary phases and then which rock types belong to the magmatic differentiation trends.

Are Li-micas primary phases? Munoz (1971) experimentally studied the stability of polylithionite and trilithionite (F-analogues) in the presence of H_2O. At 2 kbars P_{fluid}, polylithionite melted congruently at 770° ± 15 °C, while at 1 kbar it melted incongruently (to sanidine + liquid) at about 740 °C. At 2 kbar P_{fluid} the trilithionite composition melted incongruently (to eucryptite + liquid) at about 680 °C while below 1.6 kbar it broke down to eucryptic + leucite + kalsilite. Rieder (1971) experimentally studied micas on the siderophyllite–polylithionite join at 2 kbar. Although the maximum stabilities of siderophyllite and polylithionite were found to be low (about 570° and 550 °C, respectively; but contrast the latter value with data of Munoz, 1971), solid solutions containing 25–40% polylithionite were found to be stable to above 800 °C.

Tuttle and Bowen (1958) studied the effect of water pressure on melting relations in the granite system (Qtz–Ab–Or) and determined minimum melting temperatures of 720 °C at 981 bars and 685 °C at 1961 bars. The late-stage granites of

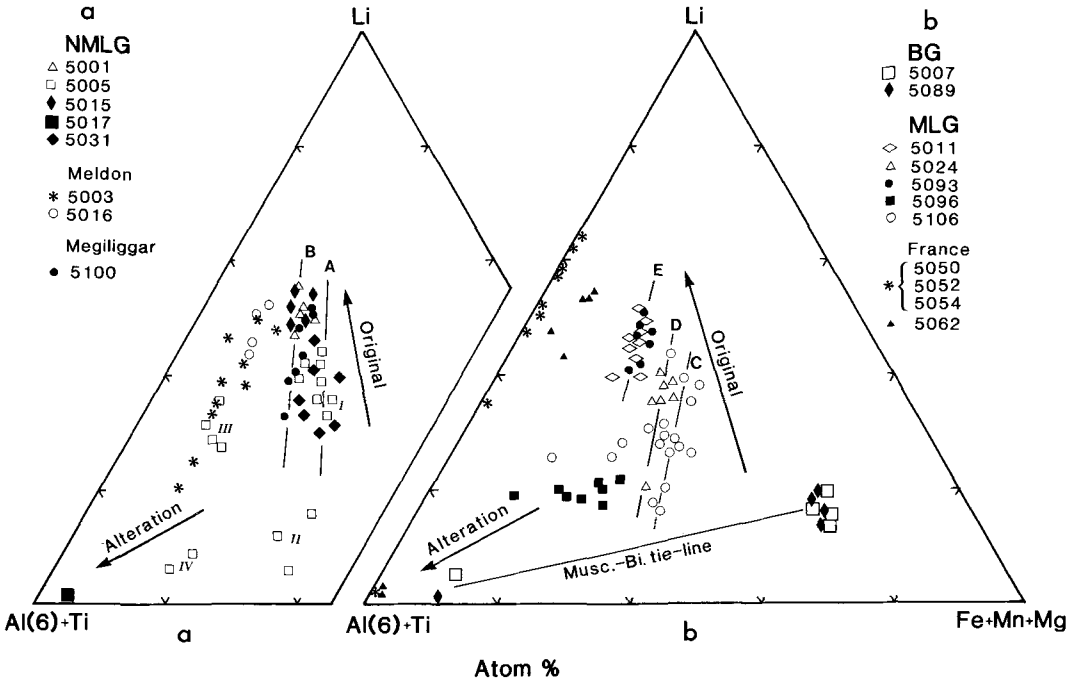

FIG. 9. Li–(Al + Ti)–(Fe + Mn + Mg) octahedral site occupancy plot (atomic) for microprobe spot analyses. The original and alteration trends are shown by arrows. For both the MLG and NMLG, intra-sample original variation trends (dashed lines labelled A–E) show greater decreases in Al than in R^{2+} as Li increases. These trends for different samples are sub-parallel and overlap to define broad inter-sample trends showing greater decreases in R^{2+}. The tie-line joins primary muscovite and biotite in the BG.

S.W. England are characteristically enriched in elements which would decrease melting temperatures further. Typical concentration ranges (Exley and Stone, 1982; Martin, 1983) for fresh Li-mica granites are (wt.%): F 0.9–2.5; Li 0.1–0.4; B 0.04–0.27; P 0.18–0.6; Rb 0.1–0.22; Cs 0.02–0.03. Experimental work has been carried out on the granite system in the presence of most of these elements—mainly at 1 kbar P_{fluid}. The main effects on liquidus and solidus temperatures at 1 kbar can be summarized as follows. Manning (1981) and Manning and Henderson (1981) have shown that F reduces minimum melting temperatures to 690 °C, 1 wt.% F; 670 °C 2% F; 630 °C 4% F. In the presence of 4% F, solidus temperatures are reduced to at least 550 °C. Martin and Henderson (1984) found minimum melting temperatures of 700 °C, 1% Li_2O; 675 °C, 2% Li_2O. Pichavant (1987) reported minimum melting temperatures of 690 °C, 1% B_2O_3; 630 °C; 4.5% B_2O_3 while Chorlton and Martin (1978) found that the solidus for a synthetic granite was decreased to 600 °C at 5% B_2O_3. Henderson and Manning (1984) reported preliminary results of the effect of Cs on phase relations for a Tuttle and Bowen 1 kbar minimum melting composition ($Qz_{38}Ab_{33}Or_{29}$). They showed that F-free charges containing 10 wt.% pollucite ($CsAlSi_2O_6$) run at 650 °C consisted mainly of glass. Further work (unpublished) places the liquidus at ~710 °C and the solidus at ~500 °C (pollucite crystallizes at ~620 °C). Rb would be expected to have a similar effect on melting relations. Finally, the results of Wyllie and Tuttle (1964) show that at 2.75 kbar the presence of ~2 wt.% P_2O_5 lowers the liquidus of a granite from ~670 °C (P-free) to ~645 °C. Manning *et al.* (1984) predicted that if such elements interact with melts by different mechanisms, as seems likely, their effects on melting temperatures could be additive.

In the experimental work reviewed above, the effect of excess Al_2O_3 (peraluminous) was not considered. Burnham and Nevkasil (1986) reported that the 4-phase eutectic point sanidine + quartz + melt + vapour at 2 kbars occurs at 767 °C while in the presence of 3.5% Al_2SiO_5 it is depressed to 737 °C. Experimental work on peraluminous natural rocks enriched in the characteristic suite of volatile and trace elements also yields significant information. Thus Burnham and Nev-

kasil (1986) discussed the experimental results for the Harding pegmatite, New Mexico [Al/(Na + K + Ca)(molar) 1.41; F 0.64 wt.%, Li_2O 0.65%, P_2O_5 0.13%, Rb_2O 0.19%, Cs_2O 0.05%]. Liduidus and solidus temperatures are 750 °C and 565 °C, respectively at 1 kbar P_{fluid}. Weidner and Martin (1987) determined the phase relations of a fluorite granite from Slip quarry, St Austell (grid reference SX 951 555) [Al/(Na + K + Ca) 1.30; F 1.15 wt.%, Li_2O 0.11%, P_2O_5 0.36%]. At 1 kbar P_{fluid} they found that the liquidus was above ~750 °C and that the solidus occurred at 660 °C; an aluminous mica (called muscovite) was stable up to 725 °C. Webster *et al.* (1987) studied a glassy rhyolite from Spor Mountain, Utah [Al/(Na + K + Ca) 1.0; F 1.2%; P_2O_5 0.06%; similar rocks from Spor Mountain (Christiansen *et al.*, 1984) contain 80–100 ppm Li; 600–1450 ppm Rb; ~60 ppm Cs]. Under water-saturated conditions at 1 kbar they found the liquidus at ~720 °C and solidus at 500 °C. Finally, London (1987) obtained some particularly fascinating experimental results for a natural glass from Macusani, Peru [Al/(Na + K + Ca) 1.5; F 1.31%, P_2O_5 0.55%, B_2O_3 0.62%, Li 1590 ppm, Rb 1150 ppm, Cs 590 ppm]. Under water-saturated conditions at 2 kbars the liquidus occurs at ~650 °C and the solidus at as low as ~450 °C. White mica (called 'muscovite') was stable up to 625 °C.

The above review shows that granite melts highly enriched in F, Li, Rb, Cs (and B) could exist down to about 500–550 °C at 1 kbar P_{fluid}. It is clear that Li-rich micas are capable of crystallizing directly from the melt i.e. they are possible primary phases. Thus we conclude that the zinnwaldite and lepidolite micas from the NMLG crystallized as primary phases and that the 'original' trends described earlier are the primary magmatic trends. It is equally clear, based on the experimental data and on the evidence of Li-mica replacement textures in some rocks (cf. Stone, 1975), that Li-mica crystallization can continue into the sub-solidus region. A separate fluid phase almost certainly existed during the final magmatic crystallization stages of the Li-mica granites, leading inevitably to subsequent auto-metasomatic recrystallization processes.

A substantial amount of work has been done on fluid inclusions in rocks from various evolutionary stages of the S.W. England batholith. Alderton and Rankin (1983) found homogenization temperatures (no pressure correction applied) up to ~570 °C for 'unaltered' biotite granite and up to ~500 °C for 'unaltered' Li-mica granite. Jackson *et al.* (1977) and Charoy (1981) studied greisens from Cligga Head. Homogenization temperatures range up to about 420 °C and require a pressure correction as the effects of boiling are rarely present. Charoy (1981) has modelled the original fluids as having a temperature of ~470 °C. Thus it seems that the temperature conditions of the latest stages of magmatic activity are essentially continuous with the onset of hydrothermal processes. Indeed, London (1987) observes that vapour and melt phases for analogous compositions (rare metal pegmatites) "may be nearly, if not completely, miscible". Under these conditions late-stage phases like Li-micas would be expected to continue crystallization sub-solidus.

At this stage we conclude that the original Li-micas in St Austell NMLG, in the Meldon aplite and in the Megiliggar Rocks phase of the Tregonning granite are all primary. In the French granites, textural relations of Li-mica in the Montebras granite indicate that it too is primary while in the Beauvoir granite they indicate that it is a secondary, sub-solidus phase.

Is the fluorite granite a primary rock type? Weidner and Martin (1987) have suggested that a fluorite granite from Slip quarry, St Austell granite (see above for analytical summary) is a primary magmatic rock type—at variance with Manning and Exley's (1984) conclusion. Weidner and Martin based their conclusion on an experimental study of a Slip chinastone sample and on a discussion of whether the Ca necessary for hydrothermal fluorite formation could be derived from albitization of BG plagioclase as suggested by Manning and Exley (1984).

It is quite clear from our petrographic and microprobe studies that an alteration series can be identified within the NMLG with the so called fluorite granites representing the most altered types. Intermediate stages of alteration of primary Li-micas have been described in which localized alteration leads to progressive loss of Li and F (also Rb, Cs) leading ultimately to Li- and F-poor or Li- and F-free muscovite micas. During the intermediate stages, F lost from the mica structure is localized mainly as fluorite growing along mica cleavages (cf. Manning and Exley, 1984). After the Li-mica has broken down completely, most of the fluorite is present as separate grains ('hard-purple chinastones').

Weidner and Martin (1987) identify the mica in their rock from Slip quarry as 'muscovite'. We have studied an altered NMLG (chinastone) from the nearby Prosper quarry (sample 5005). The bulk composition of 5005 is (all wt.%) SiO_2 72.6, TiO_2 0.04, Al_2O_3 16.1, ΣFe as Fe_2O_3 0.37, MgO 0.09, MnO 0.05, CaO 0.86, Na_2O 4.2, K_2O 5.1, P_2O_5 0.65, F 1.14, Li_2O 0.11, Rb 0.1. This rock composition is generally very similar to that

studied by Weidner and Martin and the Li and F contents are virtually identical. As shown earlier, sample 5005 shows remnant Li-mica with different populations of variously altered micas. We suggest that the Slip sample is also a hydrothermally altered rock, its relatively high Li_2O content (0.11 wt.%) perhaps suggesting the presence of some unaltered, or partially altered Li-rich micas. Thus the enhanced stability of the 'muscovite' mica phase in Weidner and Martin's (1987) experiments could be due to it containing F, as predicted by Weidner and Martin, but also the presence of Li could play a crucial role in raising the stability of the aluminous mica (cf. Munoz, 1984). Weidner and Martin conclude that if F is responsible for raising the mica stability this shows that the F/(F + OH) content of muscovite coexisting with fluorite cannot be as low as Manning and Exley (1984) had reported (0.06). Our detailed microprobe study confirms the results of Manning and Exley. It should be noted that Weidner and Martin (1987) report that fluorite is always the first phase to disappear above the solidus. Indeed their phase diagram shows that the solidus and fluorite-out curves are experimentally indistinguishable. Thus the F released from the breakdown of fluorite would have been distributed between the melt phase and the stable mica. It is to be expected that F would be distributed differently between lower-temperature, sub-solidus muscovite and fluorite and higher-temperature, super-solidus aluminous mica and F-containing silicate melt. Thus a difference between the F-level of mica deduced from Weidner and Martin's experiments and that analysed in altered rocks (Manning and Exley and this work) would be expected.

Origin of the megacrystic Li-mica unit. Manning and Exley (1984) accounted for the variability of the rock types outcropping within the MLG unit as reflecting variable degrees of metasomatism of an initial, multiply intruded biotite granite unit. Despite the pervasive alteration, unchanged BG relics remained (e.g. in Goonbarrow). Hill and Manning (1987) subsequently identified a number of primary Li-mica granite types within the MLG unit. We believe that our microprobe study confirms the latter interpretation.

As discussed earlier, the biotite from BG 5089 (Goonbarrow, i.e. within the MLG outcrop) is compositionally indistinguishable from that in BG from the main outcrop (5007, Luxulyan). BG 5089 was sampled from close to two samples of typical tourmaline-bearing MLG (5011, 5093) which contain lepidolite Li-micas. In Gunheath pit, tourmaline-free NMLG samples with lepidolite (samples 5001, 5015) and MLG with zoned (Fe, Mg)-rich zinnwaldites (5106) have been described. The latter sample shows no textural evidence of the Li-mica having formed by alteration of original biotite. The supposed large-scale, pervasive Li-metasomatism would have had to be particularly localized to account for such different mica compositions within Goonbarrow and Gunheath. The 'original' inter-sample compositional trends for the NMLG and MLG (Fig. 9) overlap, with the MLG samples being generally less evolved (less Li-rich) than their equivalent NMLG types. We believe that all these relationships are consistent with the MLG unit containing magmatic intermediates between BG and NMLG, as originally suggested by Exley (1959). Thus the 'original' mica trends described earlier for the MLG unit (including the associated biotite granites) are believed to be primary with the compositional series 5089 → 5106 → 5024 → 5011, 5093 representing increasing magmatic evolution. Compositional evolution might be expected in other phases believed to be primary and is shown by brown tourmaline in the rock series 5089→ 5106 → 5093 showing decreasing MgO (3.6 → 1.2 wt.% → below detection) and increasing FeO (11.6 → 14.0 → 15.0 wt.%).

The field relations and variable textural nature of the rock types exposed within the MLG outcrop could reflect intrusion of different pulses of magma from depth in the differentiating pluton. In addition, the presence of megacrystic types with coarse-, medium- and fine-grained groundmasses could simply reflect localized loss of vapour phases causing, in effect, pressure quenches of residual magma leading to finer grained groundmasses (cf. Manning and Hill, in press).

We conclude that many of the textural and mineralogical features of the St Austell granites (and perhaps other bodies such as the Meldon aplite and the Tregonning–Godolphin granite) are the result of the late-stage magmatic processes being extended to particularly low temperatures due to the presence of a separate aqueous fluid phase and to the enrichment of F, Li, Rb, and Cs in the melt. The end of the magmatic stage was transitional with the onset of the hydrothermal stage leading to recrystallization, in effect autometasomatism, of the magmatic mineral assemblage so introducing further textural and mineralogical complexities into the rocks.

Acknowledgements

We thank English China Clays International and Goonvean and Rostowrack China Clay Co for giving permission to visit their quarries in the St Austell granite and to collect samples. We also thank Dr J. V. P. Long

for use of the ion probe at the Department of Earth Sciences, University of Cambridge, J. S. M. acknowledges the tenure of an NERC Research Studentship. We are grateful to an anonymous reviewer, Dr D. A. C. Manning, and Prof. J. Zussman for making numerous suggestions for improving this paper.

References

Alderton, D. H. M. and Rankin, A. H. (1983) The character and evolution of hydrothermal fluids associated with the kaolinized St Austell granite, S.W. England. *J. Geol. Soc. London* **140**, 297–309.

Al-Saleh, S., Fuge, R. and Rea, W. J. (1977) The geochemistry of some biotites from the Dartmoor granite. *Proc. Ussher Soc.* **4**, 37–48.

Aubert, G. (1969) Les coupoles granitiques de Montebras et d'Échassières et la genèse de leurs minéralisations. *Mem. B.R.G.M.* (France) **46**, 332 pp.

Banner, A. E. and Stimpson, B. F. (1974) A combined ion probe/spark source analysis system. *Vacuum* **24**, 511–7.

Burnham, C. W. and Nevkasil, H. (1986) Equilibrium properties of granite magma melts. *Am. Mineral.* **71**, 239–63.

Černý, P. and Burt, D. M. (1984) Paragenesis, crystallochemical characteristics and geochemical evolution of micas in granite pegmatites. In *Micas* (S. W. Bailey, ed.). *Revs. in Mineralogy* **13**, 257–97.

Charoy, B. (1981) Post-magmatic processes in southwest England and Brittany. *Proc. Ussher Soc.* **5**, 101–15.

Chaudhry, M. N. and Howie, R. A. (1973*a*) Lithium–aluminium micas from the Meldon aplite, Devonshire, England. *Mineral. Mag.* **39**, 289–96.

———(1973*b*) Muscovite ('Gilbertite') from the Meldon aplite. *Proc. Ussher Soc.* **2**, 480–1.

Chorlton, L. B. and Martin, R. F. (1978) The effect of boron on the granite solidus. *Can. Mineral.* **16**, 239–44.

Christiansen, E. H., Bikun, J. V., Sheriden, M. F. and Burt, D. M. (1984) Geochemical evolution of topaz rhyolites from the Thomas Range and Spor Mountain, Utah. *Am. Mineral.* **69**, 223–36.

Dangerfield, J., Hawkes, J. R. and Hunt, E. C. (1980) The distribution of lithium in the St Austell granite. *Proc. Ussher Soc.* **5**, 76–80.

Exley, C. S. (1959) Magmatic differentiation and alteration in the St Austell granite. *Q. J. Geol. Soc. London* **14**, 197–230.

——and Stone, M. (1982) Hercynian igneous rocks. In *Igneous rocks of the British Isles* (D. S. Sutherland, ed.). J. Wiley & Sons, pp. 287–320.

Foster, Margaret D. (1960) Interpretation of the composition of lithium micas. *U.S. Geol. Surv. Prof. Paper* **354-E**, 115–47.

Hall, A. (1971) Greisenisation in the granite of Cligga Head, Cornwall. *Proc. Geol. Assoc. London* **82**, 209–30.

——(1988) The distribution of ammonium in granites from south-west England. *J. Geol. Soc. London* **145**, 37–41.

Hawthorne, F. C. and Černý, P. (1982) The mica group. In *Granitic pegmatites in Science and Industry* (P. Černý, ed.). *Mineral. Soc. Canada, Short Course Handbook* **8**, 63–98.

Henderson, C. M. B. and Manning, D. A. C. (1984) The effect of Cs on phase relations in the granite system: stability of pollucite. *Progr. Expt. Petr. (NERC)* **6**, 41–2.

Hill, P. I. and Manning, D. A. C. (1987) Multiple intrusions and pervasive hydrothermal alteration in the St. Austell granite, Cornwall. *Proc. Ussher Soc.* **6**, 447–53.

Jackson, N. J., Moore, J. McM. and Rankin, A. H. (1977) Fluid inclusions and mineralization at Cligga Head, Cornwall, England. *J. Geol. Soc. London* **134**, 343–9.

Jones, A. P. and Smith, J. V. (1984) Ion probe analysis of H, Li, B, F and Ba in micas with additional data for metamorphic amphibole, scapolite and pyroxene. *Neues Jahrb. Mineral. Mh.* 228–40.

Levillain, C. (1980) Etude statistiques des variations de la teneur en OH et F dans les micas. *Tschermaks Mineral. Petrogr. Mitt.* **27**, 209–33.

——(1981) Présence d'un polytype 2M, dans les lépidolites du granite de Beauvoir (Massif Central, France). *Bull. Minéral.* **104**, 690–3.

London, D. (1987) Internal differentiation of rare-element pegmatites: Effects of boron, phosphorus, and fluorine. *Geochim. Cosmochim. Acta* **51**, 403–20.

Long, J. V. P., Astill, D. M., Coles, J. N., Reed, S. J. B. and Charnley, N. R. (1980) A computer based recording system for high mass resolution ion-probe analysis. In *X-ray Optics and Microanalysis* (D. R. Beaman, R. E. Ogilvie and D. B. Wittry, eds.). Pendell Publishing Co., Midland, Michigan, pp. 316–21.

Manning, D. A. C. (1981) The effect of fluorine on liquidus phase relationships in the system Qz–Ab–Or with excess water at 1 kb. *Contrib. Mineral. Petrol.* **76**, 206–15.

——(1982) An experimental study of the effects of fluorine on the crystallization of granitic melts. In *Metallization Associated with Acid Magmatism* (A. M. Evans, ed.), pp. 191–203.

——(1988) Late-stage granitic rocks and mineralization in southwest England and southeast Asia. In *Recent advances in the geology of granite-related mineral deposits.* (R. P. Taylor and D. F. Strong, eds.). *Canad. Inst. Mining Metall.* **39**, 80–5.

——and Exley, C. S. (1984) The origins of late-stage rocks in the St Austell granite—a re-interpretation. *J. Geol. Soc. London* **141**, 581–91.

——and Henderson, C. M. B. (1981) The effect of addition of fluorine on liquidus phase relationships in the system Qz–Ab–Or with excess water at 1 kb. *Progr. Expt. Petrol. (NERC)* **5**, 16–23.

——and Hill, P. I. (In press) The petrogenetic and metallogenetic significance of topaz granite from the S.W. England orefield. *Ore-bearing granite systems: petrogenesis and mineralizing processes, Geol. Soc. Am. Special Paper* (H. J. Stein and J. L. Hannah, eds.).

——Martin, J. S., Pichavant, M. and Henderson, C. M. B. (1984) The effect of F, B and Li on melt struc-

tures in the granite system: different mechanisms? *Progr. Expt. Petrol. (NERC)* **6**, 36–41.

Martin, Joanna S. (1983) An experimental and field study of late-stage Li-rich granitic rocks. Ph.D. thesis, University of Manchester.

——and Henderson, C. M. B. (1984) An experimental study of the effects of small amounts of lithium on the granite system. *Progr. Expt. Petrol. (NERC)* **6**, 30–5.

Monier, G. and Robert, J-L. (1986) Muscovite solid solutions in the system K_2O–MgO–FeO–Al_2O_3–SiO_2–H_2O: an experimental study at 2 kbar PH_2O and comparison with natural Li-free white micas. *Mineral. Mag.* **50**, 257–66.

Munoz, J. L. (1971) Hydrothermal stability relations of synthetic lepidolite. *Am. Mineral.* **56**, 2069–86.

——(1984) F–OH and Cl–OH exchange in micas with applications to hydrothermal mineral deposits. In *Micas* (S. W. Bailey, ed.). *Revs. in Mineralogy* **13**, 469–93.

Pichavant, M. (1987) Effects of B and H_2O on liquidus phase relations in the haplogranite system at 1 kbar. *Am. Mineral.* **72**, 1056–70.

Rieder, M. (1970) Chemical composition and physical properties of lithium–iron micas from the Krusne hory Mts. (Erzgebirge). Part A: Chemical composition. *Contrib. Mineral. Petrol.* **27**, 131–58.

——(1971) Stability and physical properties of synthetic lithium–iron micas. *Am. Mineral.* **56**, 256–80.

Rosenberg, P. E. and Foit, F. F. (1977) Fe^{2+}–F avoidance in silicates. *Geochim. Cosmochim. Acta* **41**, 345–6.

Stone, M. (1975) Structure and petrology of the Tregonning–Godolphin granite, Cornwall. *Proc. Geol. Assoc. London* **86**, 155–70.

——(1984) Textural evolution of lithium mica granites in the Cornubian batholith. Ibid. **95**, 29–41.

——Exley, C. S. and George, M. C. (1988) Compositions of trioctahedral micas in the Cornubian batholith. *Mineral. Mag.* **52**, 175–92.

Tuttle, O. F. and Bowen, N. L. (1958) Origin of granite in the light of experimental studies in the system $NaAlSi_3O_8$–$KAlSi_3O_8$–SiO_2–H_2O. *Mem. Geol. Soc. Am.* **74**.

Webster, J. D., Holloway, J. R. and Hervig, R. L. (1987) Phase equilibria of a Be, U and F-enriched vitrophyre from Spor Mountain, Utah. *Geochim. Cosmochim. Acta* **51**, 389–402.

Weidner, J. R. and Martin, R. F. (1987) Phase equilibria of a fluorine-rich leucogranite from the St Austell pluton, Cornwall. Ibid. **51**, 1591–7.

Wilson, G. C. (1980) Ion microprobe techniques, with applications to analysis of Li in Cornish granites. Ph.D. thesis, Univ. of Cambridge (unpubl.), 245 pp.

——and Long, J. V. P. (1983) The distribution of lithium in some Cornish minerals: ion microprobe measurements. *Mineral. Mag.* **47**, 191–9.

Wyllie, P. J. and Tuttle, O. F. (1964) Experimental investigation of silicate systems containing two volatile components. Part 3: The effects of SO_3, P_2O_5, HCl and Li_2O in addition to H_2O on the melting temperature of albite and granite. *Am. J. Sci.* **262**, 930–9.

[*Manuscript received 29 September 1988; revised 23 January 1989*]

Appendix

A. *S.W. England*

(i) *St Austell granite*

1. 5007 BG Luxulyan (Grid Reference SX 053 589)
2. 5001 NMLG Gunheath (Grid Reference SX 003 567)
3. 5015 NMLG Gunheath (Grid Reference SX 003 567)
4. 5020 NMLG Gunheath (Grid Reference SX 003 567)
5. 5096 MLG Gunheath (Grid Reference SX 003 567)
6. 5106 MLG Gunheath (Grid Reference SX 003 567)
7. 5011 MLG Goonbarrow (Grid Reference SX 006 572)
8. 5089 BG Goonbarrow (Grid Reference SX 006 572)
9. 5093 MLG Goonbarrow (Grid Reference SX 006 572)
10. 5024 MLG Littlejohn (Grid Reference SW 982 573)
11. 5022 NMLG Kernick (Grid Reference SW 942 554)
12. 5031 NMLG Trevisco (Grid Reference SW 947 560)
13. 5080 NMLG Goonvean (Grid Reference SW 948 553)
14. 5081 NMLG Goonvean (Grid Reference SW 948 553)
15. 5085 NMLG Rostowrack (Grid Reference SW 952 564)
16. 5005 NMLG Prosper (Grid Reference SW 954 564)
17. 5017 NMLG Prosper (Grid Reference SW 954 564)

(ii) *Meldon*

18. 5003 Aplite (Grid Reference SX 566 920)
19. 5016 Aplite (Grid Reference SX 566 920)

(iii) *Tregonning–Godolphin granite*

20. 5100 Megiliggar Rocks (Grid Reference SW 611 266)

B. *Massif Central, France*

21. 5050 Beauvoir quarry, Échassières granite
22. 5052 Beauvoir quarry, Échassières granite
23. 5054 Beauvoir quarry, Échassières granite
24. 5062 Montebras granite